Astronomy & Astrophysics manuscript no. paper
April 23, 2007

Multidimensional supernova simulations with approximative neutrino transport

II. Convection and the advective-acoustic cycle in the supernova core

L. Scheck[1], H.-Th. Janka[1], T. Foglizzo[2], and K. Kifonidis[1]

[1] Max-Planck-Institut für Astrophysik, Karl-Schwarzschild-Straße 1, D-85741 Garching, Germany
[2] Service d'Astrophysique, DSM/DAPNIA, CEA-Saclay, 91191 Gif-sur-Yvette, France

received; accepted

ABSTRACT

Performing two-dimensional hydrodynamic simulations including a detailed treatment of the equation of state of the stellar plasma and of the neutrino transport and interactions, we investigate here the interplay between different kinds of non-radial hydrodynamic instabilities that can play a role during the postbounce accretion phase of collapsing stellar cores. The convective mode of instability, which is driven by the negative entropy gradients caused by neutrino heating or by variations of the shock strength in transient phases of shock expansion and contraction, can be identified clearly by the development of typical Rayleigh-Taylor mushrooms. However, in cases where the gas in the postshock region is rapidly advected towards the gain radius, the growth of such a buoyancy instability can be suppressed. In such a situation the shock and postshock flow nevertheless can develop non-radial asymmetry with an oscillatory growth of the amplitude. This phenomenon was previously termed "standing (or spherical) accretion shock instability" (SASI) by Blondin et al. (2003). It is shown here that the oscillation period of the SASI observed in our simulations agrees well with the one estimated for the advective-acoustic cycle (AAC), in which perturbations are carried by the accretion flow from the shock to the neutron star and pressure waves close an amplifying global feedback loop. Moreover, we show that the SASI oscillations can be a trigger of convective instability and like the latter they lead to an increase of the average shock radius and of the mass in the gain layer. Both hydrodynamic instabilities in combination stretch the advection time of matter accreted through the neutrino-heating layer and thus enhance the neutrino energy deposition in support of the neutrino-driven explosion mechanism. A rapidly contracting and more compact nascent neutron star turns out to be favorable for explosions, because the accretion luminosity and neutrino heating are larger and the growth rate of the AAC is higher.

Key words. hydrodynamics – instabilities – shock waves – neutrinos – stars: supernovae: general

1. Introduction

Hydrodynamic instabilities play an important role in core-collapse supernovae, because on the one hand they may be crucial for starting the explosion and on the other hand they may provide a possible explanation for the observed anisotropy of supernovae. There is a growing consensus that the neutrino-driven explosion mechanism of core-collapse supernovae does not work in spherical symmetry for progenitors more massive than about $10\,M_{\odot}$. None of the recent simulations with one-dimensional (1D) hydrodynamics and a state-of-the-art description of the neutrino transport develops an explosion (Rampp & Janka 2002; Liebendörfer et al. 2001; Liebendörfer et al. 2005; Thompson et al. 2003; Buras et al. 2003, 2006a,b). However, multi-dimensional effects were recognised to be helpful. In particular it was shown that convection is able to develop below the stalled supernova shock and that it can increase the efficiency of neutrino heating significantly (Herant et al. 1994; Burrows et al. 1995; Janka & Müller 1995, 1996). Current two-dimensional (2D) simulations are thus considerably closer to the explosion threshold than 1D models (Buras et al. 2003, 2006a,b) and a successful explosion has been reported recently for an $11.2\,M_{\odot}$ progenitor (Buras et al. 2006b). In earlier 2D simulations, in which the angular size of the numerical grid was constrained to less than 180° and in simulations in which the approximative description of the neutrino transport resulted in a fast onset of the explosion, convection was dominated by rather small angular scales of several ten degrees (Janka & Müller 1994, 1996). However, in recent 2D calculations of Buras et al. (2006a,b); Scheck et al. (2004); Burrows et al. (2006, 2007), and Scheck et al. (2006, henceforth Paper I), a slower development of the explosion and the use of a full 180° grid allowed for the formation of pronounced global (dipolar and quadrupolar) modes of asymmetry.

Send offprint requests to: H.-Th. Janka
Correspondence to: thj@mpa-garching.mpg.de

The anisotropy in these models is of particular interest, as it might provide the explanation for two results from observations: Firstly, spectropolarimetry (Wang et al. 2001, 2003; Leonard et al. 2006, and references therein) revealed that a non-spherical ejecta distribution is a common feature of many core-collapse supernovae and is probably caused by the explosion mechanism itself, since the anisotropy increases if deeper layers of the ejecta are probed. In case of Supernova 1987A this non-spherical distribution of the ejecta can even be directly imaged with the Hubble Space Telescope (Wang et al. 2002). Secondly, neutron stars move through interstellar space with velocities much higher than those of their progenitors (e.g., Cordes et al. 1993; Lyne & Lorimer 1994; Hansen & Phinney 1997; Arzoumanian et al. 2002; Zou et al. 2005; Chatterjee et al. 2005; Hobbs et al. 2005), in some cases with more than 1000 km/s. It was suggested by Herant (1995) and demonstrated with hydrodynamic simulations by Scheck et al. (2004, 2006) that neutron star velocities of this magnitude can result from strongly anisotropic (in the most extreme cases "one-sided" i.e., dipole-dominated) explosions, in which the total linear momentum of the ejecta must be balanced by a correspondingly high recoil momentum of the neutron star.

In multi-dimensional simulations convective motions break the initial global sphericity and support the explosion (or bring the model closer to the explosion threshold) by transporting cool matter from the shock to the gain radius where neutrino heating is strongest and by allowing hot matter to rise and to increase the pressure behind the stalled shock. However, it is not clear whether convection can also be responsible for the development of low modes in the postshock accretion flow, as suggested by Herant (1995) and Thompson (2000). The $l = 1$ pattern studied by Herant (1995) was motivated by a perturbation analysis of volume-filling convection in a fluid sphere by Chandrasekhar (1961), who found the dipole ($l = 1$) mode to be the most unstable one. In fact, Woodward et al. (2003) and Kuhlen et al. (2003) demonstrated with three-dimensional simulations that the $l = 1$ mode dominates the convection in red-giant and main-sequence stars. Blondin et al. (2003), however, investigating an idealized setup in 2D hydrodynamic simulations, discovered that an adiabatic accretion flow below a standing shock develops a non-radial, oscillatory instability, which they termed "standing accretion shock instability" or SASI, and which is dominated by the $l = 1$ or $l = 2$ modes. This suggests that the low-mode asymmetries found to develop in supernova cores in multi-dimensional models may be caused by global instabilities different from convection. Foglizzo et al. (2006) performed a linear stability analysis for a problem that resembles the stalled shock situation in supernovae, taking into account the limited radial size of the convectively unstable layer below the shock and the finite advection of matter through this region. The latter process turns out to have a stabilising effect and can hamper the growth of convection significantly. In particular, the lowest modes are convectively unstable only if the ratio of the convective growth timescale to the advection time through the unstable layer is sufficiently small. Foglizzo et al. (2006) estimate that this may not be the case in general and support the suggestion that instabilities different from convection may be responsible for the occurrence of low-order modes of asymmetry in the postshock accretion flow.

The "advective-acoustic cycle", in short AAC (Foglizzo & Tagger 2000; Foglizzo 2001, 2002), is a promising candidate for explaining such a (SASI) instability. It is based on the acoustic feedback produced by the advection of entropy and vorticity perturbations from the shock to the forming neutron star. By means of linear stability analysis, Galletti & Foglizzo (2005) showed that due to the AAC the flow in the stalled accretion shock phase of core-collapse supernovae is unstable with respect to non-radial perturbations, and that the highest growth rates are found for the lowest degree modes (in particular for the $l = 1$ mode).

The situation studied by Blondin et al. (2003) and Galletti & Foglizzo (2005) was, however, strongly simplified compared to real supernovae. Blondin et al. (2003) observed the growth of non-radial perturbations in a flow between an accretion shock and an inner boundary, which was located at a fixed radius. The boundary conditions were taken from a stationary flow solution. Furthermore, neither a realistic description of the equation of state of the gas nor the effects of neutrinos were taken into account by Blondin et al. (2003). Improving on this, Blondin & Mezzacappa (2006) adopted an analytic neutrino cooling function (Houck & Chevalier 1992), and Ohnishi et al. (2006) in addition took into account neutrino heating and used the more realistic equation of state from Shen et al. (1998). Both groups concur in that low-mode instabilities develop also in these more refined simulations. The nature of the instability mechanism is, however, still a matter of debate. While Ohnishi et al. (2006) consider the AAC as the cause of the low-mode oscillations, Blondin & Mezzacappa (2006) argue that a different kind of instability, which is purely acoustic and does not involve advection, is at work in their simulations. Yet, the eigenmodes found in the latter simulations were also reproduced in a linear study of Foglizzo et al. (2007), who demonstrated that at least for higher harmonics the instability is the consequence of an advective-acoustic cycle. Laming (2007), finally, suggested the possibility that feedback processes of both kinds can occur and differ in dependence of the ratio of the accretion shock radius to the inner boundary of the shocked flow near the neutron star surface.

The work by Blondin & Mezzacappa (2006), Ohnishi et al. (2006), and Foglizzo et al. (2007) shows that non-radial SASI instability of the flow below a standing accretion shock occurs also when neutrinos (which could have a damping influence) are taken into account. This is in agreement with a linear stability analysis of the stationary accretion flow by Yamasaki & Yamada (2007), who included neutrino heating and cooling, and studied the influence of varied neutrino luminosities from the proto-neutron star. They found that for relatively low neutrino luminosities the growth of an oscillatory non-radial instability is favored, with the most unstable spherical harmonic mode being a function of the luminosity, whereas for sufficiently high neutrino luminosity a non-oscillatory instability grows. They attributed the former to the AAC and the latter to convection.

All these studies concentrated on steady-state accretion flows, made radical approximations to the employed neutrino physics, and considered idealized numerical setups with special boundary conditions chosen at the inner and outer radii of the considered volume. Because of these simplifications such studies are not really able to assess the importance of the different kinds of hydrodynamic instabilities for supernova explosions. The growth rates of these instabilities depend on the properties of the flow, and are thus constant for stationary flows. In real supernovae, however, the flow changes continuously, because the shock adapts to the varying mass accretion rate, the neutrino heating below the shock changes, and the proto-neutron star contracts. Therefore the growth rates also vary, and a priori it is not clear whether they will be sufficiently high for a sufficiently long time to allow a growth of some instability to the nonlinear phase on a timescale comparable to the explosion timescale (which itself can be influenced by the instability and is a priori also unknown).

The aim of this work is therefore to go some steps further in the direction of realism and to abandon the assumption of a stationary background flow. To this end we study here the growth of hydrodynamic instabilities in a "real" supernova core, i.e., we follow in 2D simulations the post-bounce evolution of the infalling core of a progenitor star as provided by stellar evolution calculations, including a physical equation of state for the stellar plasma and a more detailed treatment of the neutrino physics than employed in the previous works. The considered models were computed through the early phase of collapse until shortly after bounce by using state-of-the-art multi-group neutrino transport (Buras et al. 2003, 2006a,b). In the long-time post-bounce simulations performed by us, we then used an approximative description of the neutrino transport based on a gray (but non-equilibrium) integration of the neutrino number and energy equations along characteristics (for details of the neutrino treatment, see Scheck et al. 2006 [Paper I]). Compared to supernova simulations with a state-of-the-art energy-dependent description of the neutrino transport (in spherical symmetry see, e.g., Rampp & Janka 2002; Liebendörfer et al. 2001; Liebendörfer et al. 2005; Thompson et al. 2003, and for multi-group transport also in 2D, see, e.g., Buras et al. 2003, 2006a,b) the models presented here thus still employ significant simplifications. Such an approximative neutrino treatment must therefore be expected to yield results that can differ quantitatively from those of more sophisticated transport schemes. Nevertheless our approach is able to capture the qualitative features of the better treatments. It is certainly significantly more elaborate (and "realistic") than the schematic neutrino source terms employed by Foglizzo et al. (2007) and Blondin & Mezzacappa (2006), and the local neutrino source description (without transport) adopted by Ohnishi et al. (2006) and Yamasaki & Yamada (2007). We consider our approximation as sufficiently good for a project that does not intend to establish the viability of the neutrino-heating mechanism but which is interested mostly in studying fundamental aspects of the growth of non-radial hydrodynamic instabilities in the environment of supernova cores including the influence that neutrino cooling and heating have in this context.

We made use of one more approximation that reduces the complexity of our simulations compared to full-scale supernova models, namely, we did not include the neutron star core but replaced it by a Lagrangian (i.e., comoving with the matter) inner grid boundary that contracts with time to smaller radii, mimicking the shrinking of the cooling nascent neutron star. At this moving boundary the neutrino luminosities produced by the neutron star core were imposed as boundary conditions. This had the advantage that we could regulate the readiness of a model to explode or not explode, depending on the size of the chosen core luminosities and the speed of the boundary contraction. Because the inner boundary of our computational is impenetrable for the infalling accretion flow, similar to the rigid core of a neutron star, our boundary handling may also be more realistic and less constraining than the outflow boundary employed by Blondin et al. (2003), Blondin & Mezzacappa (2006), and Ohnishi et al. (2006). Our modeling approach therefore follows Scheck et al. (2004) and Paper I, where indeed the development of low-mode flow (with dominant $l = 1$ and $l = 2$ modes) between shock and neutron star was found. In these previous papers we, however, did not attempt to identify the mechanism(s) that were causal for the observed phenomenon and just mentioned that convection and the acoustically-driven or AAC-driven SASI may yield an explanation for the large global asymmetries seen to develop during the neutrino-heating phase of the stalled shock. There was no analysis which mechanism was active and why it had favorable conditions for growth.

In the present work we return to these questions. In particular we aim here at exploring the following points:

- What is the timescale for a non-radial instability of the stalled accretion shock (SASI) to develop in a supernova core? How is it influenced by neutrino effects?
- Can the instability be identified as consequence of an amplifying advective-acoustic cycle, of a growing standing pressure wave (Blondin & Mezzacappa 2006) or of something else?
- What determines its growth rate? For which conditions does the instability grow faster than convection and which influence may this have on the subsequent (nonlinear) evolution?
- What is the relationship between convection and the instability in the nonlinear phase?
- What is the possible supportive role of the SASI in the context of neutrino-driven explosions and in creating the low-mode ejecta asymmetry identified as cause of large neutron star kicks by Scheck et al. (2004) and Scheck et al. (2006).

In order to address these questions we will first summarise the most important properties of convection and of the AAC in the gain layer in Sect. 2. This will serve us as basis for the later analysis of our set of two-dimensional simulations. In Sect. 3 we will describe the computational methods and numerical setup we use for these simulations and will motivate our choice of parameter values for the considered models. We will present the simulation results in Sect. 4 and will discuss them in detail in Sects. 5 and 6. Section 7, finally, contains our conclusions.

2. Hydrodynamic instabilities

2.1. Linear and nonlinear convective growth of perturbations

In a hydrostatic, inviscid atmosphere, regions with negative entropy gradients (disregarding possible effects of composition gradients) are convectively unstable for all wavelengths. Short wavelength perturbations grow fastest, with a local growth rate $\omega_{\rm buoy} > 0$ equal to the imaginary part of the complex Brunt-Väisäla frequency:

$$\omega_{\rm buoy} \equiv \sqrt{-a_{\rm grav}\, C\,/\,\rho}. \tag{1}$$

Here $a_{\rm grav} < 0$ is the local gravitational acceleration, ρ is the density and

$$C \equiv \left(\frac{\partial\rho}{\partial S}\right)_{P,Y_l} \cdot \frac{{\rm d}S}{{\rm d}r}, \tag{2}$$

where S is the entropy, P is the pressure, and Y_l is the total lepton number per nucleon. Note that $C > 0$ is the instability condition for Schwarzschild convection.

Foglizzo et al. (2006) pointed out that in the stalled shock phase, the convective growth timescale $\omega_{\rm buoy}^{-1}$ in the unstable layer below the shock is of the same order as the timescale for advection from the shock to the gain radius,

$$\tau_{\rm adv}^{\rm g} \equiv \int_{R_{\rm g}}^{R_{\rm s}} \frac{{\rm d}r}{|v_r(r)|}, \tag{3}$$

where $R_{\rm g}$ is the gain radius, $R_{\rm s}$ the shock radius and v_r the radial velocity. Advection is stabilising because it gives perturbations only a finite time to grow in the gain region, before they are advected into the stable layer below the gain radius. Considering the local growth rate $\omega_{\rm buoy}(r)$ given by Eq. (1) in a reference frame advected with the flow, the amplitude δ of a small-wavelength perturbation may grow during its advection from the shock to the gain radius, at best by a factor $\exp(\chi)$,

$$\delta_{\rm gain} = \delta_{\rm shock}\, \exp(\chi), \tag{4}$$

where the quantity

$$\chi \equiv \int_{R_{\rm g}}^{R_{\rm s}} \omega_{\rm buoy}(r)\, \frac{{\rm d}r}{|v_r(r)|} = \tau_{\rm adv}^{\rm g}/\tau_{\rm conv} \tag{5}$$

can be interpreted as the ratio of the advection timescale to the average local growth timescale the perturbation experiences, $\tau_{\rm conv} \equiv \langle\omega_{\rm buoy}^{-1}\rangle$ (the latter quantity is implicitly defined by Eq. 5). Thus it would appear that in order to reach a given perturbation amplitude at the gain radius, a certain seed perturbation amplitude of the matter crossing the shock would be necessary.

However, a linear stability analysis reveals that the stationary accretion flow below the shock is globally unstable and perturbations can grow from *arbitrarily* small initial seeds, if sufficient time is available (Foglizzo et al. 2006). According to Foglizzo et al. (2006) this is the case for a limited range $[l_{\rm min}, l_{\rm max}]$ of modes for which χ exceeds a critical value χ_0,

$$\chi > \chi_0\,, \quad \text{where} \quad \chi_0 \approx 3. \tag{6}$$

For $\chi < \chi_0$ the flow remains linearly stable, even though a negative entropy gradient is present.

The analysis of Foglizzo et al. (2006) applies only for the linear phase of the instability, i.e. for small perturbation amplitudes. However, it is possible that the situation has to be considered as nonlinear right from the beginning, i.e. that the seed perturbations grow to large amplitudes already during their advection to the gain radius. In this context "large" can be defined by considering the buoyant acceleration of the perturbations.

For a small bubble, in which the density ρ is lower than the one of the surrounding medium, $\rho_{\rm surr}$, the convective growth during the advection to the gain radius may lead to an increase of the relative density deviation $\delta \equiv |\rho - \rho_{\rm surr}|/\rho_{\rm surr}$ (which can be considered as the perturbation amplitude) as given by Eq. (4). The bubble experiences a buoyant acceleration $|a_{\rm grav}|\,\delta$ towards the shock, which is proportional to the local gravitational acceleration $a_{\rm grav}$. The time integral of the buoyant acceleration becomes comparable to the advection velocity, when the perturbation amplitude reaches a critical value

$$\delta_{\rm crit} \equiv \frac{\langle|v_r|\rangle_{\rm gain}}{\langle a_{\rm grav}\rangle_{\rm gain}\, \tau_{\rm adv}^{\rm g}} \tag{7}$$

$$\sim \frac{\langle|v_r|\rangle_{\rm gain}^2}{R_{\rm s}\,\langle a_{\rm grav}\rangle_{\rm gain}}\, \frac{R_{\rm s}}{R_{\rm g} - R_{\rm s}} \sim O(1\%)\,, \tag{8}$$

where $\langle|v_r|\rangle_{\rm gain}$ and $\langle a_{\rm grav}\rangle_{\rm gain}$ are the average values of the radial velocity and the gravitational acceleration in the gain layer, respectively. For $\delta_{\rm gain} > \delta_{\rm crit}$ a small-scale perturbation is able to rise against the accretion flow. If the whole flow is perturbed, the buoyant motions on small scales affect the situation globally and could allow for the onset of convective overturn also on larger scales. Note that in contrast to the linear growth of the instability this process does not require $\chi > \chi_0$ but it does require sufficiently large seed perturbations,

$$\delta_{\rm shock} > \frac{\delta_{\rm crit}}{\exp(\chi)}\,. \tag{9}$$

A sufficient condition for the suppression of convection is therefore that neither Eq. (6) nor Eq. (9) are fulfilled.

2.2. The advective-acoustic cycle

A second hydrodynamic instability has recently been recognised to be of potential importance in the stalled shock phase. Blondin et al. (2003) noticed that the stalled accretion shock becomes unstable to non-radial deformations even in the absence of entropy gradients, a phenomenon termed SASI. It can be interpreted as the result of an "advective-acoustic cycle" (in short AAC), as first discussed by Foglizzo & Tagger (2000) in the context of accretion onto black holes, and later studied for supernovae by Galletti & Foglizzo (2005) and Foglizzo et al. (2007) by means of linear stability analysis. The explanation of these oscillations is based on the linear coupling between advected and acoustic perturbations due to flow gradients.

Although this linear coupling occurs continuously throughout the accretion flow from the shock to the neutron star surface, some regions may contribute more than others to produce a pressure feedback towards the shock and establish a

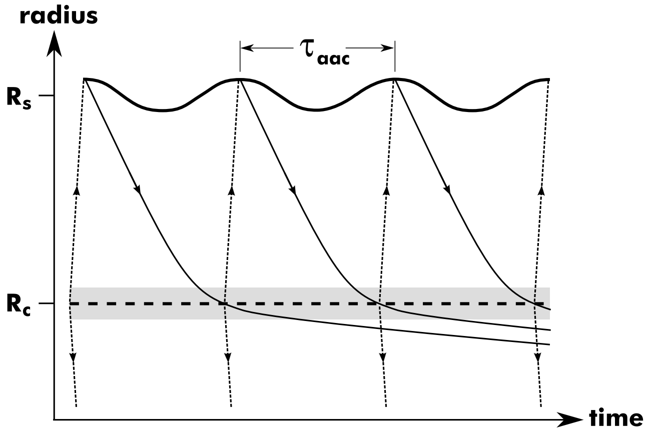

Fig. 1. Schematic view of the advective-acoustic cycle between the shock at R_s (thick solid line) and the coupling radius, R_c (thick dashed line), in the linear regime, shown for the case where the oscillation period of the shock (τ_{osc}) equals the cycle duration, τ_{aac}. Flow lines carrying vorticity perturbations downwards are drawn as solid lines, and the pressure feedback corresponds to dotted lines with arrows. In the gray shaded area around R_c the flow is decelerated strongly.

global feedback loop. The analysis of the linear phase of the instability in Sect. 5 reveals the importance of a small region at a radius R_c above the neutron star surface, where the flow is strongly decelerated. The feedback loop can be described schematically as follows: small perturbations of the supernova shock cause entropy and vorticity fluctuations, which are advected downwards. When the flow is decelerated and compressed above the neutron star surface, the advected perturbations trigger a pressure feedback. This pressure feedback perturbs the shock, causing new vorticity and entropy perturbations. Instability corresponds to the amplification of perturbations by a factor $|Q_{aac}| > 1$ through each cycle.

The duration τ^f_{aac} of each cycle is a fundamental timescale. It corresponds to the time needed for the advection of vortical perturbations from the shock to the coupling radius R_c, where the pressure feedback is generated, plus the time required by the pressure feedback to travel from this region back to the shock.

The oscillatory exponential growth resulting from the AAC can be described by a complex eigenfrequency $\omega = \omega_r + i\omega_i$ satisfying the following equation:

$$\exp(-i\omega\tau^f_{aac}) = Q_{aac}, \tag{10}$$

where the real part ω_r is the oscillation frequency and the imaginary part ω_i is the growth rate of the AAC. Note that Eq. (10) is a simplified form of Eq. (49) of Foglizzo (2002). For the sake of simplicity, it neglects the marginal influence of the purely acoustic cycle of pressure waves trapped between the shock and the accretor. This hypothesis is motivated by the recent estimate of the efficiencies Q_{aac}, $\mathcal{R}_{ac}$ of the advective-acoustic and of the purely acoustic cycles, respectively, obtained by Foglizzo et al. (2007) in a simpler set-up when the frequency is high enough to allow for a WKB approximation. According to their Figs. 8 and 9, the purely acoustic cycle is always stable ($|\mathcal{R}_{ac}| < 1$), whereas the advective-acoustic cycle is unstable ($|Q_{aac}| > 1$). According to Eq. (10), the oscillation period $\tau_{osc} \equiv 2\pi/\omega_r$ of the AAC depends both on the duration τ^f_{aac} of the cycle and on the phase φ of Q_{aac}:

$$\omega_r\tau^f_{aac} + \varphi = 2n\pi, \tag{11}$$

where n is an integer labelling the different harmonics. In the particular flow studied by Foglizzo et al. (2007), the oscillation period of the fundamental mode is a good estimate of the duration of the cycle ($\tau_{osc} \sim \tau^f_{aac}$). This simple relationship is not obvious a priori. For example, if Q_{aac} were real and negative, the oscillation period would scale like $\tau_{osc} \sim 2\tau^f_{aac}$ (because enhancing feedback requires a phase coherence between the amplifying mechanism and the shock oscillation).

The amplitude of perturbations in the AAC increases like $\exp(\omega_i t)$, with a growth rate ω_i deduced from Eq. (10):

$$\omega_i \equiv \frac{\ln(|Q_{aac}|)}{\tau^f_{aac}}. \tag{12}$$

Comparing Eqs. (5) and (12) it is interesting to note that a small advection timescale suppresses the growth of entropy-driven convection whereas it leads to higher growth rates for the AAC (neglecting the logarithmic dependence on Q_{aac}). Thus the AAC may operate under conditions which are not favourable for convection and vice versa. Investigating this further is one of the goals of this work.

3. Numerical setup and models

In order to investigate the importance of instabilities like the ones discussed in the previous section during the post-bounce evolution of core-collapse supernovae, we performed a series of two-dimensional (2D) hydrodynamic simulations. For this purpose we used the same numerical setup as in Paper I. We employed the version of the hydrodynamics code that was described by Kifonidis et al. (2003). It is based on the piecewise parabolic method (PPM) of Colella & Woodward (1984), assuming axisymmetry and adopting spherical coordinates (r, θ). The calculations were performed on a polar grid that had typically 800 zones in radial direction and 360 zones in lateral direction (extending from polar angle $\theta = 0$ to $\theta = \pi$). The lateral grid was equidistant while the radial grid had logarithmic spacing with a ratio of radial zone size to radius that did not exceed 1%. For the neutrino number and energy transport we applied a gray, characteristics-based transport scheme that was able to efficiently approximate the transport in the transparent and semi-transparent regimes up to optical depths of several 100. Only transport in the radial direction was taken into account, but we allowed for lateral variations of the neutrino flux by solving one-dimensional transport equations independently for all discrete polar angles of the r-θ grid. A detailed description of the transport method is given in Paper I.

3.1. Initial and boundary conditions

We used an initial model (the 'W' model from Paper I) that was obtained by evolving the 15 $M_\odot$ supernova progenitor s15s7b2 of Woosley & Weaver (1995) through collapse and core bounce until shock stagnation in a simulation with a detailed, energy-dependent treatment of neutrino transport (Buras et al. 2003;

Table 1. Important quantities for the simulations discussed in this paper. $L_{\rm ib}$ is the constant boundary luminosity, $R^{\rm f}_{\rm ib}$ the asymptotic inner boundary radius (see Eq. 13), $t_{\rm ib}$ the contraction timescale of the inner boundary, $\delta_{\rm i}$ the amplitude of the initial velocity perturbations (which was chosen to be proportional to the local radial velocity v_r in most cases — see text for details), $L_{\nu_{\rm e}+\bar\nu_{\rm e}}$ is the luminosity of electron neutrinos and antineutrinos at a radius of 500 km at 150 ms after the start of the simulations, $t_{\rm nl}$ the time at which the average lateral velocity in the gain layer exceeds 10^9 cm/s, $\Delta M_{\rm gain}$ the mass in the gain layer at the time $t_{\rm exp}$ when the explosion starts, $E_{\rm exp}$ the explosion energy, $M_{\rm ns}$ the neutron star mass, and $v_{\rm ns}$ the neutron star velocity as computed from momentum conservation. The last three quantities are given at $t = 1$ s, for Model W00F at $t = 750$ ms, and $t_{\rm exp}$ is defined as the moment when the energy of the matter in the gain layer with positive specific energy exceeds 10^{49} erg. Model W00FA is a hydrodynamic simulation without including neutrino effects. Only Models W00F, W12F, and W12F-c developed explosions and values for the corresponding explosion and neutron star parameters are given. The neutrino luminosities imposed at the inner boundary are kept constant during a time $t_L = 1$ s. The energy unit 1 B = 10^{51} erg is used and all times are measured from the start of the simulation, i.e. $t = 0$ s means 16 ms after core bounce.

Name	$L_{\rm ib}$ [B/s]	$R^{\rm f}_{\rm ib}$ [km]	$t_{\rm ib}$ [s]	$\delta_{\rm i}$	$L_{\nu_{\rm e}+\bar\nu_{\rm e}}$ [B/s]	$t_{\rm nl}$ [s]	$t_{\rm exp}$ [s]	$\Delta M_{\rm gain}$ [$M_\odot$]	$E_{\rm exp}$ [B]	$M_{\rm ns}$ [$M_\odot$]	$v_{\rm ns}$ [km/s]
W00FA	–	8.0	0.5	$10^{-3}\,v_r$	0.0	–	–	–	–	–	–
W00F	0.2	8.0	0.5	$10^{-3}\,v_r$	99.0	0.154	0.194	0.004	0.37	1.50	200
W00	0.2	15.0	1.0	$10^{-3}\,v_r$	51.7	0.346	–	–	–	1.63	−3
W00S	0.2	15.0	4.0	$10^{-3}\,v_r$	29.6	–	–	–	–	–	–
W05S	7.4	15.0	4.0	10^6cm/s	38.3	–	–	–	–	–	–
W05V	7.4	15.0	10.0	3×10^7cm/s	33.5	–	–	–	–	–	–
W12F	29.7	10.5	0.25	$10^{-3}\,v_r$	109.3	0.144	0.164	0.010	0.87	1.44	−558
W12F-c	29.7	10.5	0.25	$\mathcal{O}(10^{-2})\,v_r$	112.5	0.090	0.117	0.015	0.94	1.41	612

see their Model s15). We started our runs at a time of 16 ms after core bounce. In order to enable the growth of hydrodynamic instabilities we perturbed the initial model, unless noted otherwise, by adding random, zone-to-zone velocity perturbations of 0.1% amplitude.

The neutron star core (i.e. typically the innermost 1.1 $M_\odot$) was not included in our simulations but was replaced by a contracting inner boundary of the computational grid. Boundary conditions were imposed there for the hydrodynamics and the neutrino transport, and a point-mass potential of the excised core was adopted to account for the gravitational influence of this region. Although the treatment of gravity is not of primary relevance for the fundamental questions studied in this paper, we mention here that the description of the gravitational potential took into account the self-gravity of the gas on the grid with its two-dimensional distribution, as well as an approximative treatment of general relativistic effects (for details, see Paper I).

The inner grid boundary was placed at a Lagrangian shell with enclosed mass of $M = 1.1\,M_\odot$ at which we imposed conditions describing hydrostatic equilibrium. Its radius was assumed to evolve according to

$$R_{\rm ib}(t) = \frac{R^{\rm i}_{\rm ib}}{1 + (1 - \exp(-t/t_{\rm ib}))\,(R^{\rm i}_{\rm ib}/R^{\rm f}_{\rm ib} - 1)}\,, \qquad (13)$$

where $R^{\rm f}_{\rm ib}$ is the final (asymptotic) boundary radius, $t_{\rm ib}$ is the contraction timescale and $R^{\rm i}_{\rm ib} \approx 65$ km is the initial radius, which is given by the initial model. The neutrino luminosities from the neutron star core, which we imposed at the inner boundary, were assumed to be constant during the first second after core bounce. This simple choice can be justified by the results of core-collapse simulations with sophisticated neutrino transport (see Paper I).

With this approach we parametrized the cooling and shrinking of the core of the nascent neutron star and its neutrino emission, which all depend on the incompletely known properties of the nuclear equation of state. Different choices of the boundary motion and strength of the neutrino emission allowed us to vary the properties of the supernova explosion.

In some of the simulations discussed here, the rapid contraction of the forming neutron star caused the density and sound speed at the inner boundary to become so high that the hydrodynamic timestep was severely limited by the Courant-Friedrich-Lewy (CFL) condition. Moreover, when the optical depth in this region increased to more than several hundred, numerical problems with our neutrino transport method occurred unless very fine radial zoning was chosen, making the timestep even smaller. In such cases we moved the inner grid boundary to a larger radius and bigger enclosed mass (i.e., we increased the excised neutron star core). Hereby we attempted to change the contraction behavior of the nascent neutron star as little as possible. The new inner boundary was placed at a radius $R'_{\rm ib}$ where the optical depth for electron neutrinos was typically around 100. When doing this, the gravity-producing mass of the inner core was adjusted appropriately (e.g., Arcones et al. 2006) and the boundary neutrino luminosities were set to the values present at $R'_{\rm ib}$ at the time of the boundary shifting, thus making sure that the gravitational acceleration, the neutrino flux, and neutrino heating and cooling above $R'_{\rm ib}$ followed a continuous evolution. The parameters in Eq. (13) were adjusted from the old values $R^{\rm i}_{\rm ib}$ and $R^{\rm f}_{\rm ib}$ to new values $\widetilde{R}^{\rm i}_{\rm ib}$ and $\widetilde{R}^{\rm f}_{\rm ib}$, respectively, in the following way:

$$\begin{aligned} \widetilde{R}^{\rm i}_{\rm ib} &= R^{\rm i}_{\rm ib} \times (R'_{\rm ib}/R_{\rm ib})\,, \\ \widetilde{R}^{\rm f}_{\rm ib} &= R^{\rm f}_{\rm ib} \times (R'_{\rm ib}/R_{\rm ib})\,. \end{aligned} \qquad (14)$$

This simple rescaling had the consequence that during the subsequent evolution small differences of the contraction velocity of the new inner boundary and therefore of the settling neutron star appeared, which led also to minor changes of the decay

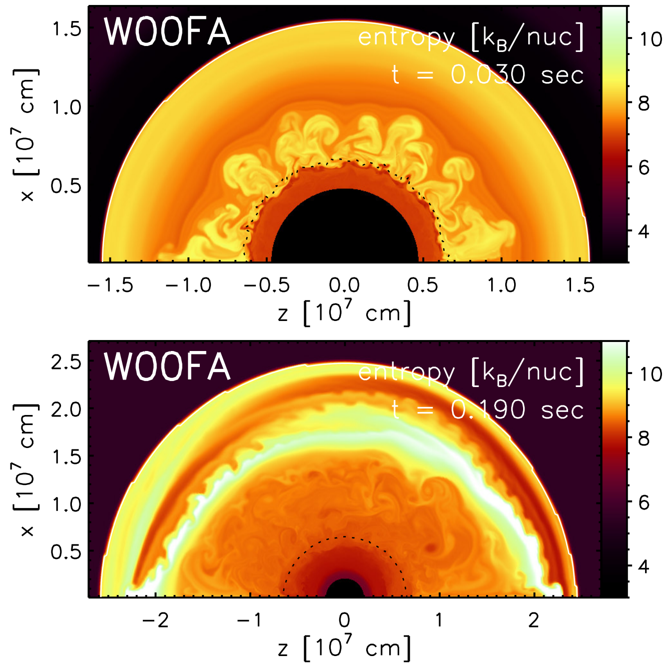

Fig. 2. Entropy distribution of model W00FA 30 ms and 190 ms after the start of the simulation. The initial entropy profile and postshock entropy gradients caused by shock motions give rise to weak convection. A low-amplitude $l = 1$ oscillation develops.

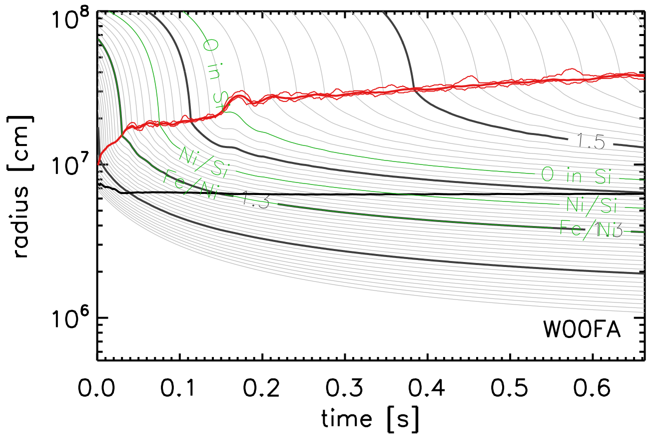

Fig. 3. Mass-shell trajectories for model W00FA. The spacing of the thin lines is 0.01 $M_\odot$. Green lines mark the mass shells at which the composition of the progenitor changes. The red lines are the minimum, average, and maximum shock radii, the black line marks the radius, at which the average density is 10^{11} g/cm^3. The difference between minimum and maximum shock radius is caused by bipolar shock oscillations (see Fig. 2).

of the neutrino luminosities with time. Nevertheless, no significant impact on the simulations was observed, e.g., Model W00F developed an explosion at the same time, independent of whether or not the boundary was shifted according to our recipe.

3.2. Model parameters

The characteristic parameters and some important quantities of the eight models investigated here are listed in Table 1. The models differ concerning the included physics, assumed boundary conditions, and the initial perturbations used to seed the growth of hydrodynamic instabilities.

The most simplified case we considered, Model W00FA, is a purely hydrodynamic simulation without including neutrino effects. This choice follows Blondin et al. (2003), who also ignored neutrinos. In comparison with the other models we computed, it allows us to study the influence of neutrino cooling and heating. Blondin et al. (2003) also placed an inner boundary at a fixed radius and applied outflow conditions there to allow for a steady-state accretion flow. In contrast, in Model W00FA accretion is enabled by the retraction of the inner boundary of the computational grid, which mimics the Lagrangian motion of a mass shell in a contracting neutron star. Another difference from Blondin et al. (2003) is the fact that in our models the accretion rate varies when infalling matter from the less dense layers at increasingly larger radii reaches the shock. Thus the development of hydrodynamic instabilities occurs in a situation that is generically non-stationary.

In five other simulations we included neutrinos and chose boundary conditions such that the growth of convection was suppressed. This allowed us to identify and study other instabilities like the SASI more easily. The suppression of convection could be achieved by prescribing vanishing or negligibly low core luminosities. In such cases only the luminosity produced between the inner boundary and the gain radius causes neutrino energy deposition in the gain layer. Therefore the neutrino heating remains weak, resulting in a shallow entropy gradient and consequently in a large growth timescale for convection. This implies that for low core luminosities the ratio of the advection to the buoyancy timescale, χ (Eq. 5), remains below the critical value and therefore in spite of a negative entropy gradient in the neutrino heating region, the postshock layer remains convectively stable due to the rapid advection of the gas down to the gain radius (see Sect. 2.1). The five simulations where this is the case are Models W00F, W00, W00S, W05S, and W05V. These models differ in the prescribed contraction of the inner boundary. Models W00 and W00F employ the "standard" and "rapid" boundary contraction, respectively, of Paper I. In order to cover a wider range of advection timescales — which will help us to gain deeper insight into the mechanism that causes the low-mode instability found in our simulations (see Sect. 5) — we performed three simulations with slower boundary contraction, namely Models W00S, W05S, and W05V (Table 1). In the last two models the core neutrino luminosity has a non-negligible (but still fairly low) value. The correspondingly enhanced neutrino heating leads to larger shock radii and thus longer advection timescales. Models W00F, W00, and W00S were computed with our standard initial perturbations (0.1% random noise on the velocity). For Models W05S and W05V an $l = 1$ velocity perturbation was applied. This allowed us to suppress high-mode noise and to measure the oscillation period of the low-mode instability despite the low growth rates in these models.

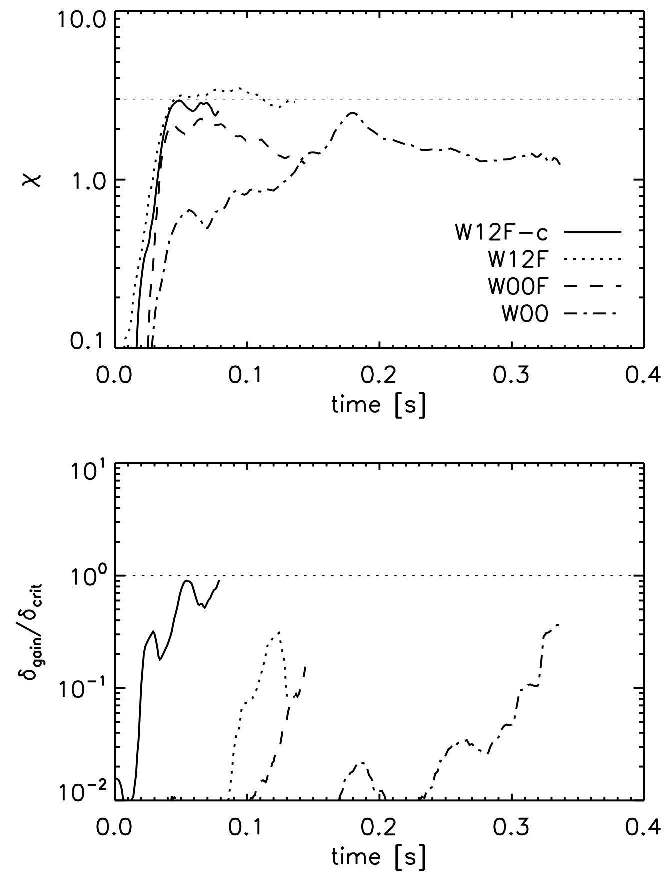

Fig. 4. Evolution of the quantity χ (upper panel, see Eq. 5) and of the ratio $\delta_{\rm gain}/\delta_{\rm crit}$ (lower panel, see Eqs. 4, 8) for Models W12F-c, W12F, W00F and W00. All lines end 10 ms before the nonlinear phase begins at time $t_{\rm nl}$, when the average lateral velocity in the gain layer exceeds 10^9 cm/s. At later times χ and $\delta_{\rm crit}$ cannot be measured reliably any longer. In all models, $\chi \lesssim \chi_0 \approx 3$ at $t < t_{\rm nl}$. Only in Model W12F-c the ratio $\delta_{\rm gain}/\delta_{\rm crit}$ gets very close to unity before $t = t_{\rm nl}$, which means that only in this model convection is able to set in faster than the SASI.

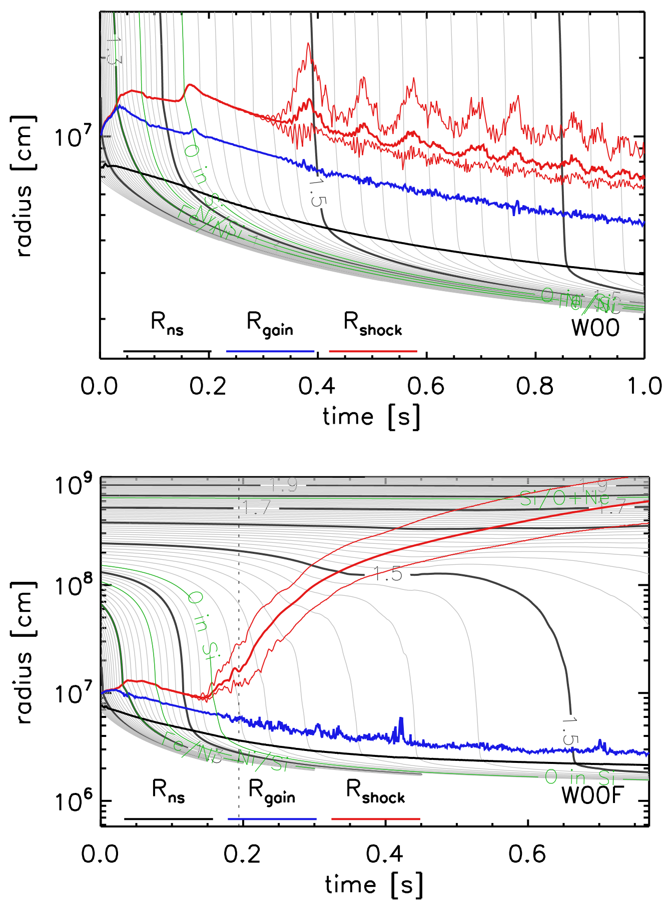

Fig. 5. Same as Fig. 3, but for Models W00 (upper panel) and W00F (lower panel). The blue line marks the position of the gain radius. Up to $t \approx 300$ ms Model W00 remains nearly spherical and evolves like the corresponding one-dimensional simulation. However, an initially very weak $l = 1$ oscillation mode in the postshock flow grows in this phase and finally becomes nonlinear, causing strong shock oscillations. Yet, this model does not explode. Although the shock expands transiently in a quasi-periodic manner, the average shock radius decreases and all matter remains bound. In Model W00F an $l = 2$ mode develops and starts to affect the shape of the shock at $t \approx 150$ ms, much earlier than in Model W00. The oscillations become nonlinear, and at $t = 194$ ms (marked by a dotted vertical line) the model explodes.

For Models W12F and W12F-c, finally, we adopted boundary conditions that were guided by core-collapse simulations with sophisticated multi-group neutrino transport. The contraction of the inner boundary was chosen to match the motion of the corresponding mass shell in such simulations for the same progenitor (Buras et al. 2003). The boundary luminosity we imposed led to typical explosion energies of about 10^{51} erg. Despite the non-negligible core luminosity convection in these models was suppressed because of the rapid boundary contraction. The latter caused the radius of the stalled shock to become rather small, and consequently the accretion velocities in the postshock layer were very large. Therefore the advection timescale was short and the parameter χ did not exceed the critical value of about 3. In such a situation the amplitude of the progenitor perturbations can decide about whether convection sets in (starting in the nonlinear regime as discussed in Sect. 2.1) or not. Since the properties of the perturbations in the progenitor star are not well known, we decided to explore two cases, one (Model W12F) with small initial perturbations (our standard 0.1% velocity perturbation) such that the growth of convection was suppressed, and another case where the initial perturbations were sufficiently large so that convection could develop. For the latter model, W12F-c, we used the same perturbations as for Models W12-c and W18-c of Paper I with amplitudes of up to several percent and a spatial variation as given by the velocity fluctuations that had grown during a 2D core-collapse simulation of a 15 $M_\odot$ star (Model s15r of Buras et al. 2003 and Buras et al. 2006b).

4. Results

In this section we will give an overview of the simulation results whose interpretation will be given in more detail in Sects. 5 and 6.

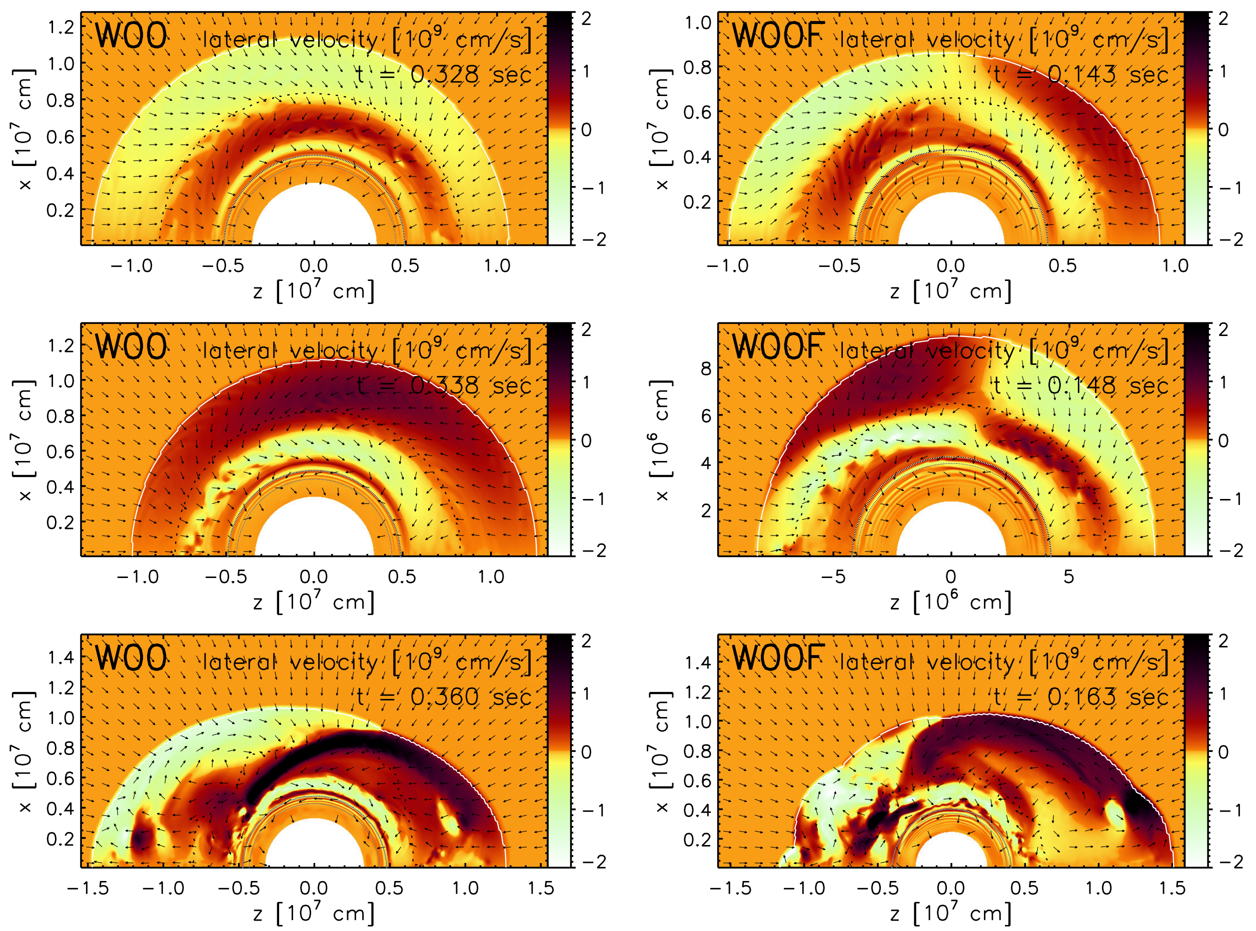

Fig. 6. Lateral velocities (color coded; superimposed are the vectors of the velocity field, which indicate the direction of the flow) for Models W00 and W00F. The white lines mark the shock, the black dotted lines the gain radius. For both models we show the situation at two times near $t = t_{\rm nl}$, at which the oscillations are in opposite phases (i.e. the times differ by half an oscillation period), and at a third time, when the oscillations have run out of phase (see Sect. 6.1). In Model W00 an $l = 1$ SASI mode develops, i.e., the still nearly spherical shock moves back and forth along the z-axis, whereas in Model W00F an $l = 2$ SASI mode becomes dominant, i.e., the shock oscillates between a prolate and an oblate deformation. The postshock matter attains high lateral velocities, because the radial preshock flow hits the shock at an oblique angle when the shock is nonspherical or when its center is displaced from the grid center.

4.1. A model without neutrinos

Although Model W00FA does not include neutrino heating, convective fluid motions develop in this case because a convectively unstable region with a negative entropy gradient is present at $r \approx 70$ km already in the initial conditions of our simulations. This feature is a consequence of the decreasing shock strength before shock stagnation. Soon after we start model model run W00FA, buoyant bubbles form in the unstable region and rise towards the shock (Fig. 2). Convective action continues during the whole simulation because neutrino cooling, which could damp convection, is disregarded, and because convectively unstable entropy gradients are created by shock motions that are caused by variations of the preshock accretion rate and by bipolar shock oscillations due to SASI modes (see Sect. 6.1). However, without neutrino heating the convective overturn does not become as strong and dynamical as in the simulations of Paper I, where neutrino effects were included. Also the bipolar shock oscillations are rather weak (the shock deformation amplitude does not exceed 15%) and occur quasi-periodically with a period of 20–50 ms (Fig. 3).

These multi-dimensional processes do not affect the overall evolution of the model and the shock position as a function of time is almost identical to the one found in a corresponding one-dimensional simulation. In spite of the contraction of the inner grid boundary, the shock expands slowly and continuously (Fig. 3). A transient faster expansion occurs at $t \approx 150$ ms, when a composition interface of the progenitor star falls through the shock and the mass accretion rate drops abruptly. After 660 ms we stopped the simulation. At this time the shock had reached a radius of 400 km.

Although the shock expands slowly, this does not lead to an explosion because without neutrino heating the specific energy of the matter behind the shock remains negative. The shock expansion takes place because matter piles up in the postshock region and forms an extended atmosphere around the neutron star. This slowly pushes the shock further out in response to the adjustment of hydrostatic equilibrium by the accumulation of mass in the downstream region. Since in the absence of cooling

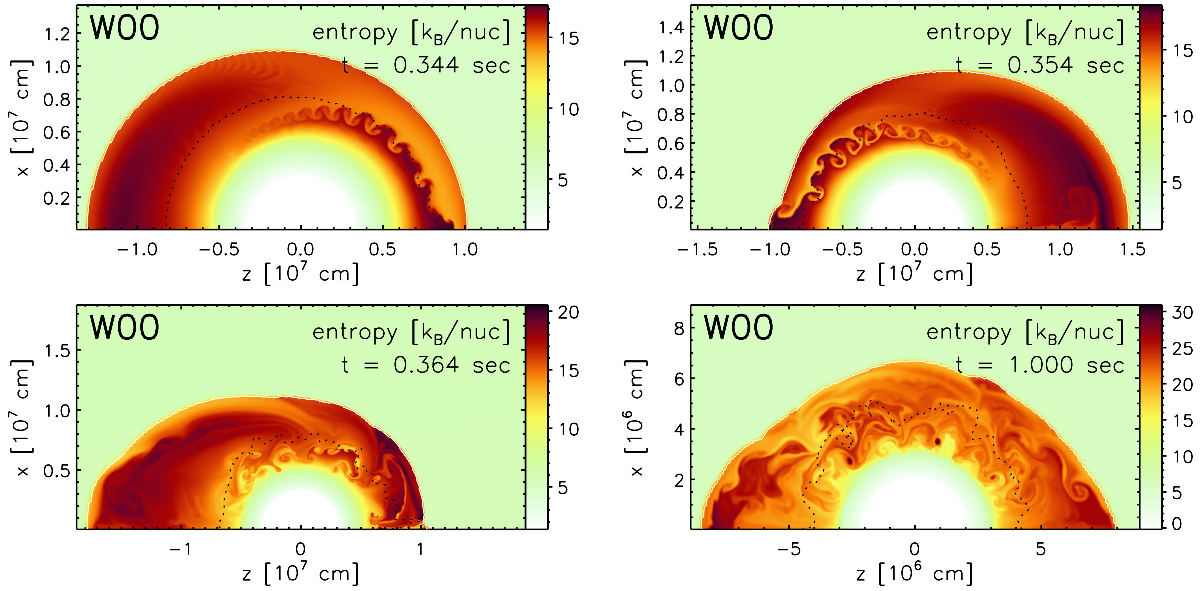

Fig. 7. Entropy distribution of Model W00 for several moments near the beginning of the nonlinear phase (the displayed times have a separation of half an oscillation period), and at $t = 1$ s. Within each SASI oscillation cycle the postshock entropies vary strongly and steep, unstable entropy gradients develop in the postshock flow. Finally, the Rayleigh-Taylor growth timescale becomes smaller than the oscillation period and the characteristic mushroom structures are able to grow. In the subsequent evolution the low-mode oscillations saturate and the model does not develop an explosion.

processes the matter cannot lose its entropy, it is not able to settle down onto the neutron star quickly. Therefore the behavior of Model W00FA is destinctively different from the situation obtained in supernova simulations with neutrino transport, and it also differs from the stationary flow that was considered by Blondin et al. (2003). The postshock velocity in Model W00FA is much lower and the shock radius becomes larger.

Neutrino cooling is therefore essential to obtain a quasi-steady state accretion flow when simulations are performed in which the central neutron star is included (in our models it is partly excised and replaced by an impenetrable inner grid boundary). Only when neutrinos remove energy and reduce the entropy of the gas can the matter be integrated into the dense surface layers of the compact object. The rapid flow of the gas from the shock to the neutron star implies short advection timescales, which are crucial for the growth of the SASI (see the discussion in Sec. 2.2). Although the accretion flow that develops in our supernova simulations is similar to the one assumed by Blondin et al. (2003) and Ohnishi et al. (2006), there are still potentially important differences. Because of the contraction of the neutron star and due to the density gradient in the collapsing star, the mass accretion rate varies with time and the accretion between shock and neutron star surface never becomes perfectly stationary. Our simulations also differ from those of Ohnishi et al. (2006) and Blondin & Mezzacappa (2006) by our more detailed treatment of the neutrino effects and by the fundamentally different inner boundary condition, which allows one to assess the question whether the use of the outflow boundary in the previous studies had any consequences for the development of non-radial shock instabilities.

4.2. Models with suppressed convection

In the models including neutrino transport the accreted matter loses energy and entropy by neutrino cooling and thus is able to settle down onto the neutron star, following the contraction of the inner boundary. Comparing the mass shell trajectories of the neutrinoless Model W00FA and of Model W00 (shown in Figs. 3 and 5, respectively) this difference becomes evident. Since the accreted matter does not pile up, also the shock turns around after an initial expansion phase and recedes continuously during the later evolution (except for a short, transient expansion phase a $t \approx 150$ ms, which is initiated when a composition interface of the progenitor star crosses the shock). Due to the miniscule boundary luminosity the neutrino heating remains weak and the parameter χ of Eq. (5) stays below the critical value (Fig. 4). Consequently, there is no evidence of convection in the gain layer and Model W00 evolves nearly spherically symmetrically in the first 300 ms.

However, already several ten milliseconds after the start of the simulation a lateral velocity component (which changes direction with a period of about 30 ms) is observable in the flow between shock and neutron star surface. The amplitude of this $l = 1$ oscillation mode starts to increase continuously after $t \approx 100$ ms and grows by a factor of about two per period. However, the amplitude is not large enough to affect the shape of the shock before $t \approx 250$ ms because the finite resolution of the numerical grid prevents the shock from being pushed out by less than one radial zone and thus it remains perfectly spherical for low oscillation amplitudes (lateral variation is already visible in the postshock flow, though).

In the subsequent evolution the shock radius is initially still slowly decreasing and the shock shape remains approximately

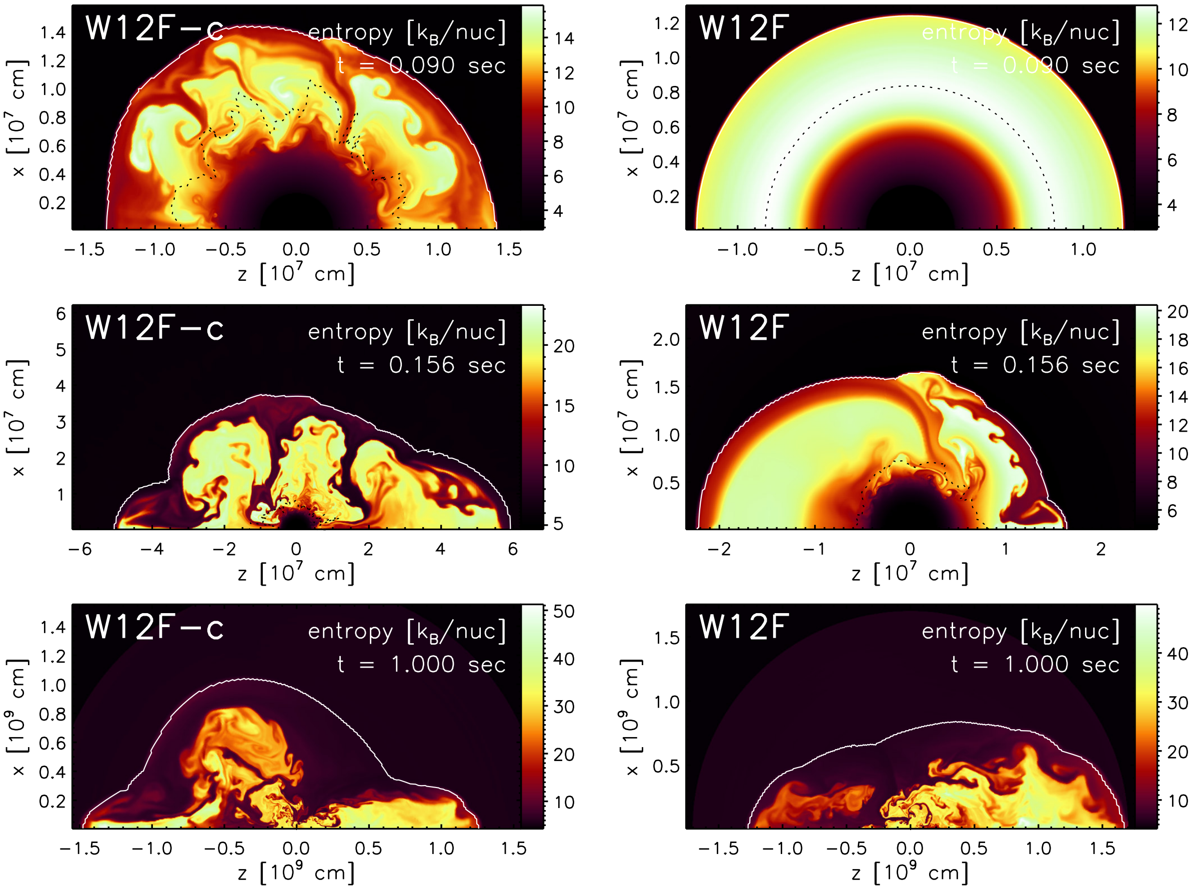

Fig. 8. Entropy distribution of Models W12F-c (left column) and W12F (right column) for several times. Model W12F-c quickly develops anisotropies because of the onset of convection, whereas in Model W12F convection is initially suppressed and low-mode SASI oscillations become visible after about 100 ms. After these oscillations have grown to large amplitude and have begun to trigger convection also in Model W12F, the two models explode in a qualitatively very similar way, although the detailed structure and asymmetry of the postshock flow and supernova shock are clearly different.

spherical, but the shock surface moves back and forth along the axis of symmetry assumed in our two-dimensional simulations. The direction of the postshock flow changes periodically and the flow transports matter between the southern and the northern hemispheres (Fig. 6). This situation is quite similar to the bipolar oscillations encountered in some models discussed in Paper I and also in full-scale supernova simulations with sophisticated neutrino transport (Buras et al. 2006b). However, because convection is absent, the flow pattern and the shape of the shock are much less structured in Model W00.

At $t \approx 360$ ms the amplitude of the shock oscillations has become very large, the shock radii at the poles differ by up to 50 km, whereas the average shock radius is only about 100 km. In this phase the entropy behind the shock starts to vary strongly with time and angle (Fig. 7). Steep negative entropy gradients ($\mathrm{d}S/\mathrm{d}r = O(1\,k_\mathrm{b}/\mathrm{km})$) develop and Rayleigh-Taylor instabilities start to grow at the boundaries between low- and high-entropy matter. The postshock flow reaches lateral velocities of several 10^9 cm/s and supersonic downflows towards the neutron star form (see Sect. 6.1 for a discussion of these processes). Within a few oscillation cycles the whole postshock flow becomes very similar to the nonlinear convective overturn present at the onset of the explosion in those models of Paper I where the explosion energy was rather low.

However, in contrast to these simulations of Paper I, Model W00 does not explode. At $t \approx 390$ ms the bipolar oscillations reach their maximum amplitude. In the further evolution they become weaker and on average the shock radius decreases (Fig. 5). The slow decay of activity is interrupted by several short phases of stronger shock expansion and bipolar oscillation, which occur quasi-periodically every 50–100 ms. When we stop the simulation at $t = 1$ s the shock has retreated to a radius of only 70 km on average.

Models W00S, W05S, and W00V, in which a slowly contracting neutron star was assumed, evolve qualitatively very similar to Model W00. However, with increasing contraction timescale the oscillation period becomes longer (up to 100 ms) and the growth rate of the low-mode instability decreases. All these models are dominated by an $l = 1$ SASI mode and none of them is able to explode.

Also Model W00F with its rapidly contracting inner boundary evolves initially quite similar to Model W00 (Fig. 5). However, all timescales are shorter: The oscillation amplitude starts to grow already after 50 ms, the shock becomes nonspherical at $t \approx 130$ ms and convection sets in at $t \approx 160$ ms.

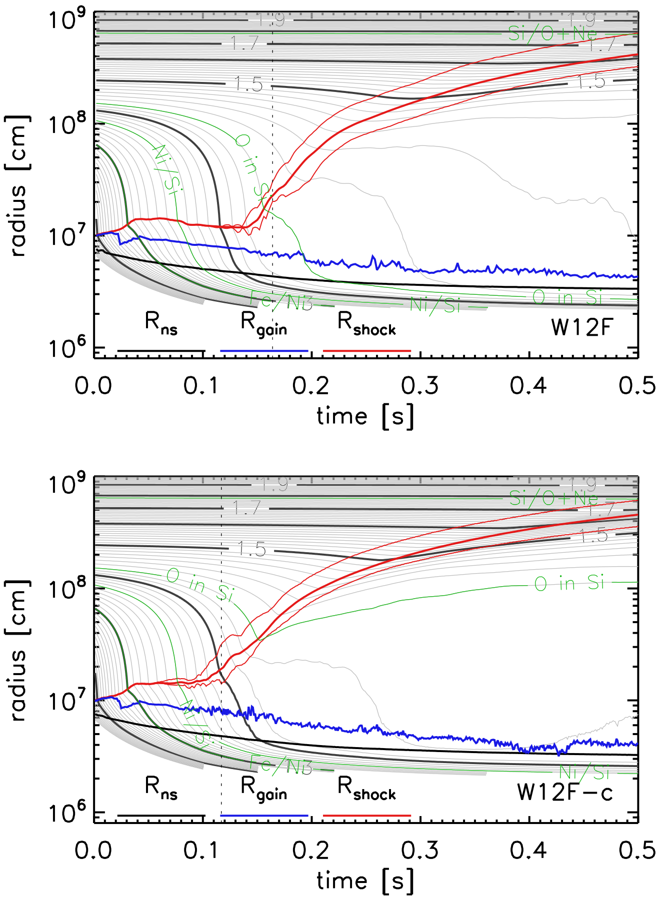

Fig. 9. *Upper panel:* Same as Fig. 5, but for Model W12F. After an initial phase, in which the model remains nearly spherically symmetric, the AAC becomes strong enough to deform the shock and to trigger convection. This model explodes at $t \approx 160$ ms (marked by the vertical dotted line), after the oxygen-enriched silicon shell is has fallen through the shock. *Lower panel:* Mass-shell plot for Model W12F-c. Convective activity starts to deform the shock in this model at $t \approx 60$ ms, and the explosion occurs already at $t \approx 120$ ms, before the oxygen-enriched silicon layer (whose inner boundary is indicated by the line labelled with "O in Si") has fallen through the shock.

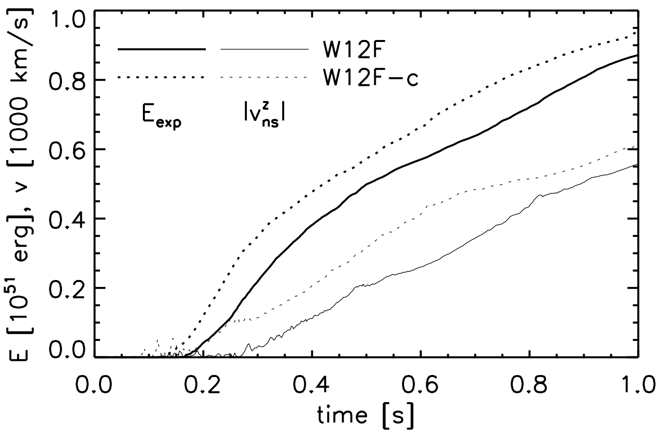

Fig. 10. Evolution of the explosion energy (thick) and the neutron star velocity (thin) for Models W12F (solid) and W12F-c (dotted).

Furthermore, Fig. 6 shows that in this model the $l = 2$ mode (i.e. oscillation between prolate and oblate states) is initially more strongly excited than the $l = 1$ mode, which starts to dominate only just before the onset of the explosion.

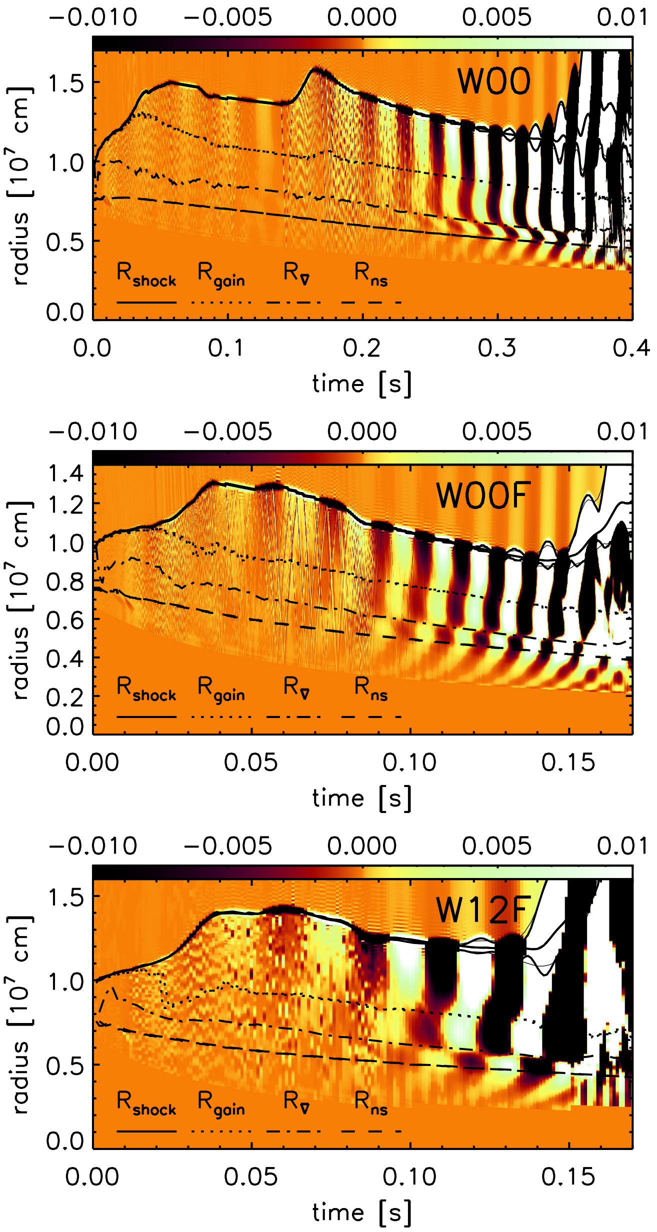

Fig. 11. Time evolution of the amplitude of the dominant spherical harmonics mode of the pressure, normalized by the amplitude of the $l = 0$ mode, as function of radius for Models W00, W00F and W12F. The solid lines are the minimum, average, and maximum shock radius, the dotted line is the gain radius, the dashed line is the neutron star surface (defined as the location where the density is 10^{11} g cm^{-3}), and the dash-dotted line marks the position, $R_\nabla(t)$, of the largest velocity gradient. A low-mode oscillation develops in the postshock flow. A pronounced phase shift is visible at a radius $R_\varphi(t)$ that agrees well with the position of the largest velocity gradient. The "noise" (short-wavelength sound waves) visible in the early phase after bounce is caused by the shock propagation and is not related to the advective-acoustic cycle.

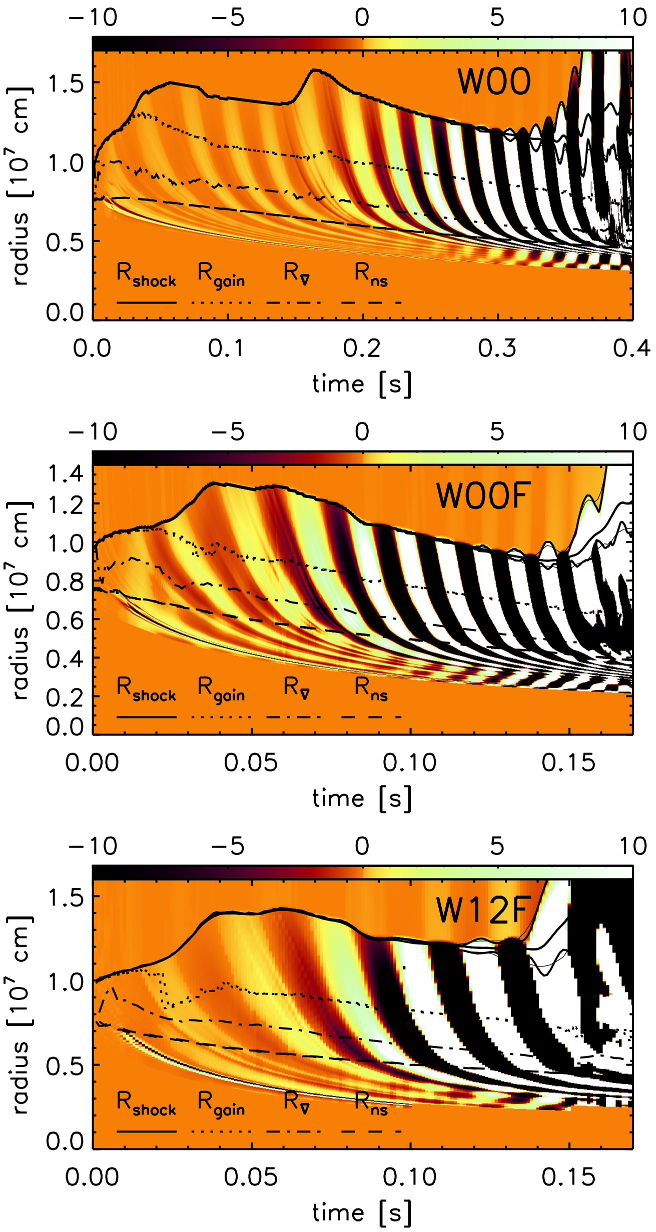

Fig. 12. Time evolution of the amplitude of the dominant spherical harmonics mode of the quantity $A(r,t,\theta)$ of Eq. (15), displayed as function of radius for Models W00, W00F and W12F. The lines have the same meaning as in Fig. 11. As in the latter figure, a zebra-like pattern becomes visible here already several ten milliseconds after bounce a zebra-like, indicating that matter with a nonvanishing lateral velocity component is advected from the shock towards the neutron star.

In contrast to the models with slower boundary contraction, the continuous neutrino heating in Model W00F is sufficiently strong to trigger an explosion at $t_{\rm exp}$ = 194 ms. This difference is caused by the fact that the faster contraction leads to gravitational energy release (the accreted matter heats up by compression) and thus to higher neutrino luminosities (see Sec. 6.2 for further discussion). The anisotropic gas distribution caused by the low-mode oscillations becomes frozen in when the shock accelerates outward. The shock develops a prolate deformation and a single accretion funnel forms in the northern hemisphere. Since the explosion develops a large-scale asymmetry, the anisotropic distribution of the ejecta exerts a strong gravitational force that causes an acceleration of the newly formed neutron star (see Paper I for details about this process and the procedure of evaluating the simulations for the resulting kick velocity of the neutron star). Due to the miniscule boundary luminosity the energy of the explosion remains rather low (0.37×10^{51} erg at 750 ms after bounce, see Table 1, and 0.5×10^{51} erg for the extrapolated value at 1 s), but the neutron star attains a fairly high kick velocity ($v_{\rm ns} \approx 200$ km/s at 750 ms post bounce and estimated 350 km/s for t = 1 s).

4.3. Models with typical explosion energies

While the simulations discussed so far demonstrate clearly the existence of a non-radial instability that is not convection, they were based on the assumption that the core neutrino luminosities are negligibly small. In contrast, in W12F and W12F-c boundary luminosities were assumed such that the explosion energies reached values close to those considered to be typical of core-collapse supernovae. An overview of the evolution these models can be obtained from Figures 8 and 9, where we show entropy distributions at several times and the mass-shell plots, respectively.

In Model W12F-c, in which large initial seed perturbations were assumed (cf. Table 1), the first convective bubbles form at $t \approx 60$ ms, and at $t \approx 90$ ms the whole gain layer has become convective (see Fig. 8). From this time on the total energy in the gain layer rises continuously and already at $t_{\rm exp} \approx 120$ ms the first zones acquire positive total energy and the model explodes. The initially weakly perturbed Model W12F behaves differently in the first 200 ms. There is no sign of convection and for the first 100 ms the shock radius evolves as in a corresponding one-dimensional model. However, as in Model W00 a weak $l = 1$ oscillation mode is present in the postshock flow already at early times ($t \approx 30$ ms) and grows exponentially to large amplitudes. At about $t_{\rm nl} \approx 150$ ms steep convectively unstable entropy gradients are generated behind the oscillating shock and within two cycle periods a situation develops that strongly resembles model W12F-c at the onset of the explosion. Also Model W12F explodes, though a bit later than Model W12F-c, at t = 164 ms.

Although the pre-explosion evolution and the explosion timescales of the two models are different, the models behave quite similar after the explosion has set in. The convective structures merge and downflows form at the interface between expanding, neutrino-heated gas and the matter with lower entropy just behind the shock. The number of downflows decreases with time and from $t \approx 200$ ms on a single downdraft dominates the anisotropic gas distribution. Its position differs in the two models, as does the shape of the shock, but the explosion energies and even the neutron star velocities grow nearly in the same way after $t \sim 0.3$ s and reach essentially the same values at the end of our simulations (Fig. 10).

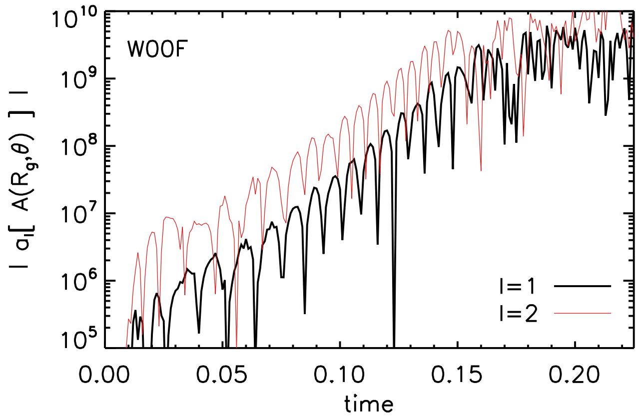

Fig. 13. Oscillatory growth of the amplitudes a_1 and a_2 of the l = 1, 2 spherical harmonics terms of the quantity $A(r, t, \theta)$ of Eq. (15) at the gain radius of Model W00F.

5. The linear phase of the instability: identification of the AAC

We now turn to a detailed investigation of the hydrodynamic instabilities that determine the evolution of the models discussed in the previous section. The projection of acoustic and advected perturbations on spherical harmonics reveals that the shock oscillations are associated with coherent pressure fluctuations and with the downward advection of perturbations produced at the shock. This association is visible in all simulated cases, and is clearly illustrated by Figs. 11 and 12 for Models W00, W00F, and W12F. In Fig. 12, advected perturbations are displayed by the amplitudes of the largest modes of the spherical harmonics of a quantity $A(r, t, \theta)$, which is particularly useful for a quantitative analysis of the AAC. It is defined as

$$A(t, r, \theta) \equiv \frac{1}{r^2 \sin\theta} \frac{\partial}{\partial\theta} \left(v_\theta(t, r, \theta) \sin\theta\right) , \qquad (15)$$

with rA being the divergence of the lateral velocity component, i.e., $A \equiv r^{-1}\mathrm{div}(v_\theta \boldsymbol{e}_\theta)$. At the gain radius, its expansion in spherical harmonics $Y_{l,m}(\theta, \phi)$ is written as

$$A(t, R_\mathrm{g}(t), \theta) = \sum_{l=0}^{\infty} a_l(t)\, Y_{l,0}(\theta, 0), \qquad (16)$$

where due to the assumption of axisymmetry only $m = 0$ has to be considered.

For $l > 0$, the spherical harmonics coefficients a_l of this quantity are proportional to the ones of the shock displacement (see Foglizzo et al. 2006, Appendix F), so $A(t, R_\mathrm{g}, \theta)$ contains basically the same information as $R_\mathrm{s}(t, \theta)$. We prefer to use $A(t, R_\mathrm{g}(t), \theta)$ rather than the shock displacement $\delta R = R_\mathrm{s}(\theta) - \langle R_\mathrm{s}\rangle_\theta$ (used in Blondin et al. 2003 and Ohnishi et al. 2006) because A is much less affected by noise ($A(t) = 0$ for a non-stationary spherical flow, whereas $R_\mathrm{s}(t)$ is varying) and allows one to measure the oscillation period and the growth rate much more sensitively than it is possible by using R_s. As an example, the absolute values of the coefficients a_1 and a_2 are shown as functions of time for Model W00F in Fig. 13.

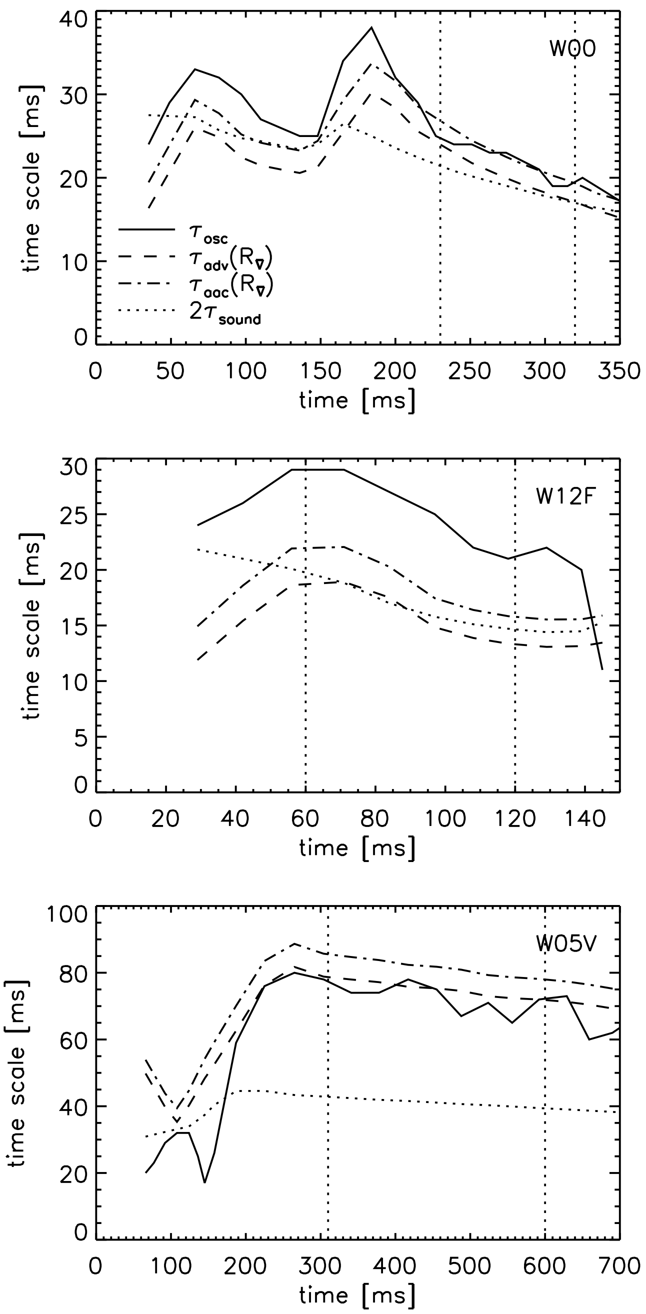

Fig. 14. Evolution of the $l = 1$ mode oscillation period, τ_osc, of the advection time from the shock to the radius of the strongest deceleration, τ^∇_adv, and of twice the sound travel time through the shock cavity, $2\tau_\mathrm{sound}$, for Models W00, W12F and W05V. While in Model W00 all timescales are similar ($\tau_\mathrm{osc} \approx \tau^\nabla_\mathrm{adv} \approx 2\tau_\mathrm{sound}$), both τ^∇_adv and $2\tau_\mathrm{sound}$ are smaller than the oscillation period in Model W12F. In Model W05V only the advection time agrees with the oscillation period, whereas $2\tau_\mathrm{sound}$ is significantly (about a factor two) smaller. The vertical dotted lines enclose the time intervals considered for the evaluations of Figs. 15 and 17.

For a given mode l the oscillation period τ_l can be determined from the minima of $|a_l(t)|$, which occur at times $t = t^n_{\mathrm{min},l}$ when n is a counter for the minima. The detection of the minima works reliably only when the amplitude is sufficiently large

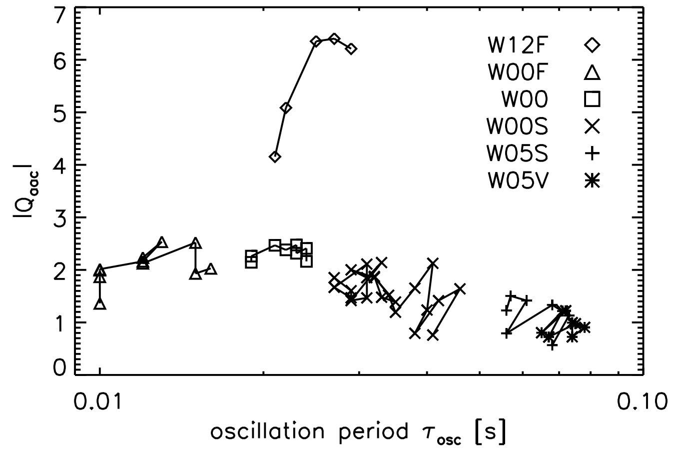

Fig. 15. Cycle efficiency, $|Q_{\mathrm{aac}}|$, as a function of the oscillation period, τ_{osc}, for Models W00F, W00, W00S, W05S, W05V and W12F.

(it therefore fails in the first 10–20 ms) and is also not feasible when convective instabilities involve a broad range of frequencies in the nonlinear phase. During one cycle of mode l the corresponding coefficient $a_l(t)$ becomes zero twice, therefore the cycle period can be measured as

$$\tau_{\mathrm{osc},l}(t^n_{\mathrm{min},l}) = t^{n+1}_{\mathrm{min},l} - t^{n-1}_{\mathrm{min},l}\,. \tag{17}$$

The evolution of the period of the $l = 1$ modes, $\tau_{\mathrm{osc},1}$, evaluated with Eq. (17), is displayed for three of our models in Fig. 14.

In order to measure the cycle efficiency, Q_{aac}, we use again the coefficients a_l defined in Eq. (16). We detect the positions of the maxima of $|a_l(t)|$, which occur at times $t = t^n_{\mathrm{max},l}$ (n now being the counter for the maxima). If the oscillations of mode l are dominated by the k-th harmonic (i.e. $\tau^k_{\mathrm{aac}} = \tau^{\mathrm{f}}_{\mathrm{aac}}/k$, where $\tau^{\mathrm{f}}_{\mathrm{aac}}$ is the period of the fundamental mode), $|a_l(t)|$ has $2k$ maxima during one fundamental cycle period $\tau^{\mathrm{f}}_{\mathrm{aac}}$, so the amplification per *fundamental* cycle can be measured as

$$Q_{\mathrm{aac},l}(t^n_{\mathrm{max},l}) = \left(\frac{a_l(t^{n+1}_{\mathrm{max},l})}{a_l(t^{n-1}_{\mathrm{max},l})}\right)^k. \tag{18}$$

This method fails, if several of the harmonics are excited with similar strength. However, these phases can be identified and typically one of the harmonics dominates clearly (mostly the fundamental mode, $k = 1$). The efficiencies measured by using Eq. (18) are shown in Fig. 15.

The pattern of the pressure perturbations in Fig. 11 reveals the presence of a particular radius R_φ where a phase shift occurs. The dash-dotted line in these figures is defined as the radius R_∇ where the velocity gradient of the unperturbed flow has a local extremum. This particular radius seems to have an important influence on the properties and behavior of pressure perturbations; in all studied cases the two radii coincide:

$$R_\nabla \sim R_\varphi\,. \tag{19}$$

This striking coincidence is likely to be the consequence of a particularly efficient coupling between advected and acoustic perturbations in layers where the accretion flow is strongly decelerated. In order to test this hypothesis, we have compared the wavelength $2\pi v/\omega_r$ (ω_r was defined in the context

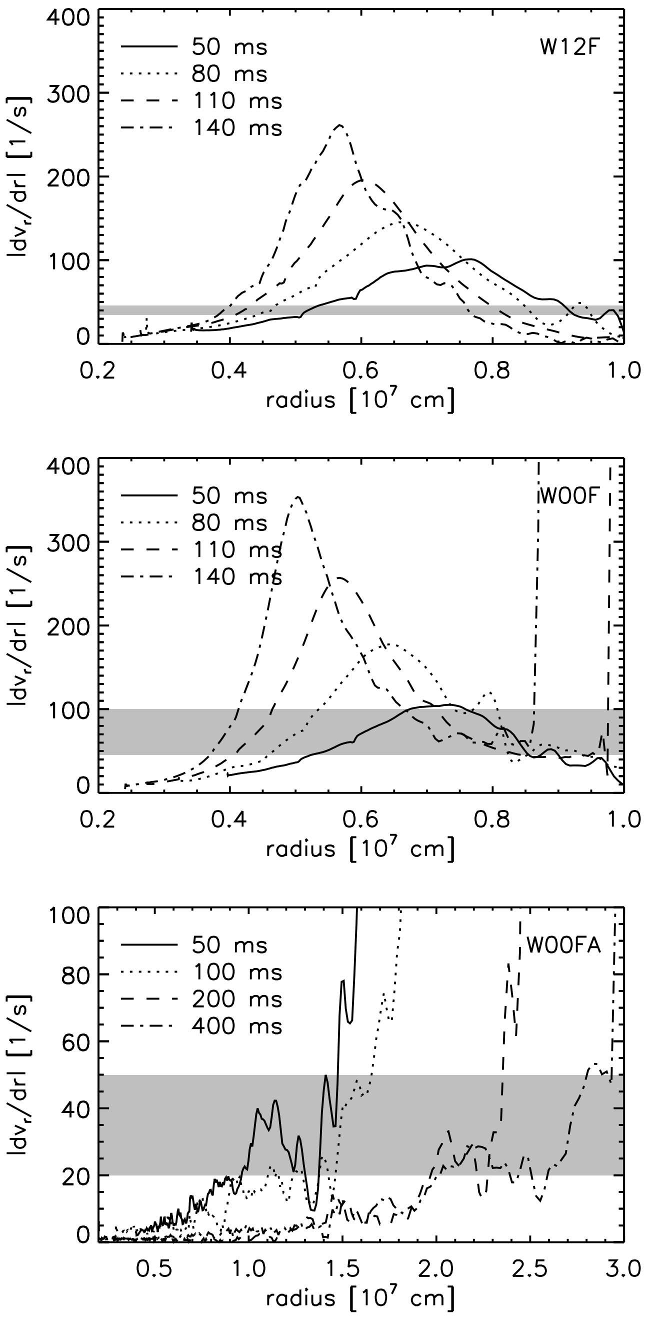

Fig. 16. Absolute values of the radial derivative of the radial velocity component as functions of radius for Models W12F, W00F, and W00FA at several times. The gray-shaded area indicates the range of values of τ^{-1}_{osc} during these times. In the models including neutrinos a pronounced "deceleration peak" forms with a maximum value significantly higher than τ^{-1}_{osc}), whereas such a feature is absent in Model W00FA.

of Eq. 10) of advected perturbations at radius R_∇ to the length scale $|\mathrm{d}\log v/\mathrm{d}r|^{-1}$ of this deceleration zone. An efficient coupling is expected if the flow velocity varies on scales shorter than the wavelength of advected perturbations:

$$\left|\frac{\mathrm{d}\ln v}{\mathrm{d}r}\right|^{-1} \lesssim \frac{2\pi v}{\omega_r} \quad\longleftrightarrow\quad \tau_{\mathrm{osc}} \gtrsim \left|\frac{\mathrm{d}v}{\mathrm{d}r}\right|^{-1}. \tag{20}$$

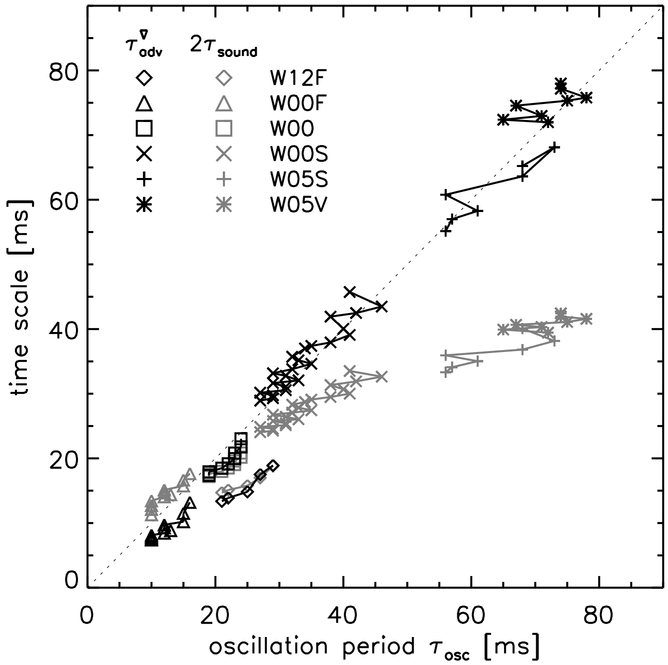

Fig. 17. Advection time τ_{adv}^{∇} of fluid moving from the shock to the radius of maximum deceleration, R_∇, and twice the sound crossing time through the shock cavity, $2\tau_{sound}$, as a function of the oscillation period, τ_{osc}, for Models W00F, W00, W00S, W05S, W05V and W12F. For the analysis of this figure only data are used from from phases in which the oscillations can be clearly identified and in which the flow is quasi-stationary (see Fig. 14). In particular the models with slow neutron star contraction yield evidence for the fact that the oscillation period scales with τ_{adv}^{∇} rather than $2\tau_{sound}$.

This hypothesis is confirmed by our simulations for Models W12F and W00F in Fig. 16. In case of the neutrinoless Model W00FA, where only a very weak SASI mode develops, a prominent deceleration peak is indeed absent. This suggests an interpretation of R_∇ as an effective coupling radius between advected perturbations and acoustic feedback:

$$R_c \equiv R_\nabla \sim R_\varphi \, . \tag{21}$$

We would like to mention that the extrema of the flow deceleration that are present in our simulations with approximative neutrino transport are also found in simulations with more sophisticated energy-dependent neutrino transport and therefore seem to be generic features of the neutrino-cooled accretion flow.

It is interesting to compare the oscillation period τ_{osc} measured for our models with the timescale τ_{aac}^{f} of the fundamental AAC mode, approximated by the advection time $\tau_{adv}(R_\nabla)$ of the fluid moving from the shock to R_∇ ($\tau_{aac}^{f} \approx \tau_{aac}^{\nabla} \approx \tau_{adv}^{\nabla}$; Fig. 14). A systematic comparison between the measured oscillation timescale, the advection timescale, and the acoustic timescale of sound waves moving through the shock cavity is shown in Fig. 17 for six of our eight models. In all models except W12F, the advection time is very close to the oscillation period, whereas in Model W12F we find $\tau_{adv}(R_\nabla) < \tau_{osc}$. In the framework of the AAC, this comparison indicates that the amplification factor Q_{aac} is real and positive in most cases, but involves a phase shift φ in case of Model W12F (cf. Eq. 11). This phase shift is indeed visible in the pressure evolution shown in the lower plot of Fig. 11 and occurs in the vicinity of the gain radius. This peculiarity is probably a consequence of the stronger neutrino heating in Model W12F, which favours the buoyancy-driven growth of perturbations in the gain layer and thus may be responsible for an additional advective-acoustic coupling near the gain radius. The presence of an additional source of amplification of the AAC in Model W12F is confirmed also by the amplification factor Q_{aac} that is displayed for six of our eight simulated models in Fig. 15. The amplification factor has modest values between 1 and 3 in most cases, whereas it is as high as $Q_{aac} \gtrsim 6$ in Model W12F. A similar effect, however less strong, is present in Model W00F, where the rapid boundary contraction leads to a significant accretion luminosity and therefore also enhanced neutrino heating in the gain layer.

In all other models the oscillation period is essentially equal to the advection time and with larger τ_{osc} increasingly longer than the sound travel time on a distance of twice the full diameter of the accretion shock cavity, $2\tau_{sound}$. The latter time is the longest characteristic timescale and thus the fundamental period on which oscillatory amplification by a purely acoustic cycle could happen. While this acoustic timescale is similar to the oscillation period τ_{osc} in Models W00F and W00, it is shorter by up to 30% in case of Model W00S and by up to a factor of two in case of Models W05S and W05V (Figs. 14 and 17). Since the oscillation period can only be equal to or smaller than the period of the fundamental mode of the driving cycle, i.e. the oscillation frequency can only be equal to the fundamental cycle frequency or an overtone of it, we interpret Fig. 17 as a clear support of our hypothesis that the SASI oscillations are a consequence of the AAC and not of a purely acoustic amplification process as suggested by Blondin & Mezzacappa (2006).

6. Interpretation of the nonlinear phase

In the following we will discuss our simulations during the nonlinear phase of the evolution in which the SASI cannot be considered as a small perturbation. In particular, we will analyse the relation between the SASI and convective instability, as well as the role these instabilities play for the explosion mechanism and the resulting energy of the explosion.

6.1. The SASI as trigger of convective overturn

In models with low core neutrino luminosity convective activity does initially not occur because the corresponding instability is suppressed in the accretion flow of the neutrino-heating layer according to Eqs. (6) and (8). The first large-scale nonradial perturbations in the postshock flow of such models are therefore caused by SASI oscillations. Once large average lateral velocities around $10^9\,\mathrm{cm\,s^{-1}}$ or more are reached in the gain layer at $t > t_{nl}$ (cf. Table 1), however, also the smaller-scale mushroom-like structures that are typical of the onset of Rayleigh-Taylor instability start to grow. Within only a few more oscillation cycles, plumes of neutrino-heated matter and supersonic downdrafts of low-entropy matter develop and violent convective overturn sets in very similar to what we found in case of the models described in Paper I. There are two effects that are mainly responsible for the corresponding change of the flow character; these are linked to the unsteady motion and the growing deformation of the shock, respectively.

Firstly, in course of radial expansion and contraction phases the shock reaches velocities of $O(10^9\mathrm{cm/s})$, which is a significant fraction of the preshock velocity. Since the postshock entropy depends on the preshock velocity in the frame of the shock, such fast shock oscillations cause strong variations of the entropy in the downstream region. Rapid outward motion of the shock produces high entropies in the postshock flow, whereas phases in which the shock retreats lead to lower postshock entropies. Periodic shock expansion and contraction thus results in alternating layers with high and low entropies, which are compressed as the accreted matter is advected towards the neutron star. With increasing amplitude of the shock oscillations the convectively unstable entropy gradients between these layers eventually become so steep that the growth timescale of Rayleigh-Taylor instabilities shrinks to about 1 ms, which is much shorter than the advection timescale. Therefore nonradial perturbations are able to grow quickly at the entropy interfaces and vortices and mushroom-like structures begin to form (see Fig. 7).

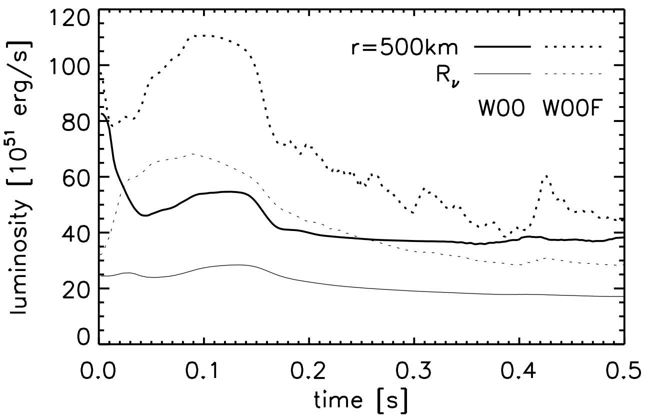

Fig. 18. Evolution of the sum of the ν_e and $\bar{\nu}_e$ luminosities at the neutrinosphere and at $r = 500\,\mathrm{km}$ for Models W00 and W00F. The luminosities decay with time because the largest mass accretion rates are present at early times ($t < 0.2\,\mathrm{s}$). Model W00F has the higher luminosity, because the neutron star contracts faster, setting free more gravitational energy.

Secondly, also the off-center displacement of the accretion shock by the $l = 1$ SASI mode and the shock deformation caused by $l \geq 2$ modes play an important role when the amplitudes become sufficiently large. The radial preshock flow hits the deformed or displaced shock at an oblique angle. Since the velocity component tangential to the shock is not changed when the gas passes through the shock, in contrast to the normal component, which is strongly reduced, the flow is deflected and attains a substantial lateral velocity component, whose size and sign changes during the cycle period, see Fig. 6. As long as the cycle amplitude is small, the lateral velocity components are also small, and the postshock flow remains approximately radial. In case of a strongly deformed shock, however, the postshock flow becomes mainly non-radial because the lateral velocity reaches a significant fraction of the preshock velocity (up to several 10^9 cm/s, i.e. the lateral flow becomes supersonic). For an $l = 1$ mode, the highest negative lateral velocities are obtained when the shock has its maximum displacement in the negative z-direction, see Fig. 6, upper left panel. A shell of matter with high negative lateral velocity formed in this phase is advected towards the neutron star, and half an oscillation period later the highest positive lateral velocities are generated right behind the shock when the shock expands into positive z-direction (Fig. 6, middle left panel). With increasing oscillation amplitude the shock radius – and consequently also the advection timescale and the cycle period – begin to vary so strongly during one cycle that the northern and southern hemispheres run "out of phase" so that the shock radii at the north pole ($\theta = 0°$) and at the south pole ($\theta = 180°$) reach their maximum values not alternatingly any more, but at almost the same time. In this case streams of matter with high positive and high negative lateral velocities emerge simultaneously near the north and south pole, respectively. These streams collide and one of them is deflected upwards, producing a bump bounded by two "kinks" in the shock surface, while the other one is directed downwards, forming a supersonic downflow (see Fig. 6, lower left panel and Fig. 8, middle right panel), a phenomenon which we have also observed in the simulations of Paper I.

Large-amplitude SASI oscillations are thus able to trigger nonlinear convective overturn even in models in which the growth of buoyancy instabilities is initially suppressed because of unfavorable conditions in the accretion flow as discussed in the context of Eqs. (6) and (8).

6.2. From SASI oscillations to explosions

Why is Model W00F able to develop an explosion while Model W00 and the models with even slower boundary contraction (W00S, W05S, W05V) do not explode? Models W00 and W00F differ in the assumed contraction of the nascent neutron star, i.e. in the parameters describing their final inner boundary radius, $R_{\mathrm{ib}}^{\mathrm{f}}$, and the contraction timescale, t_{ib}. A smaller value of $R_{\mathrm{ib}}^{\mathrm{f}}$ implies that the matter accreted on the forming neutron star sinks deeper into the gravitational potential and thus more gravitational energy is released. The smaller value of t_{ib} causes this release of energy to happen earlier. Most of the potential energy that is converted to internal energy by $p\mathrm{d}V$-work is radiated away in the form of neutrinos. Consequently, the neutrino luminosity that leads to heating in the gain layer is much higher at early times in case of Model W00F (Fig. 18).

Yet, these high luminosities alone are not sufficient to start an explosion. This is demonstrated by a one-dimensional simulation with the same boundary parameters as Model W00F, which fails to explode. It is well known that in the multidimensional case convection leads to an enhancement of the efficiency of neutrino energy deposition in the gain layer, on the one hand because non-radial convective motions stretch the time fluid elements can stay in the gain layer and are

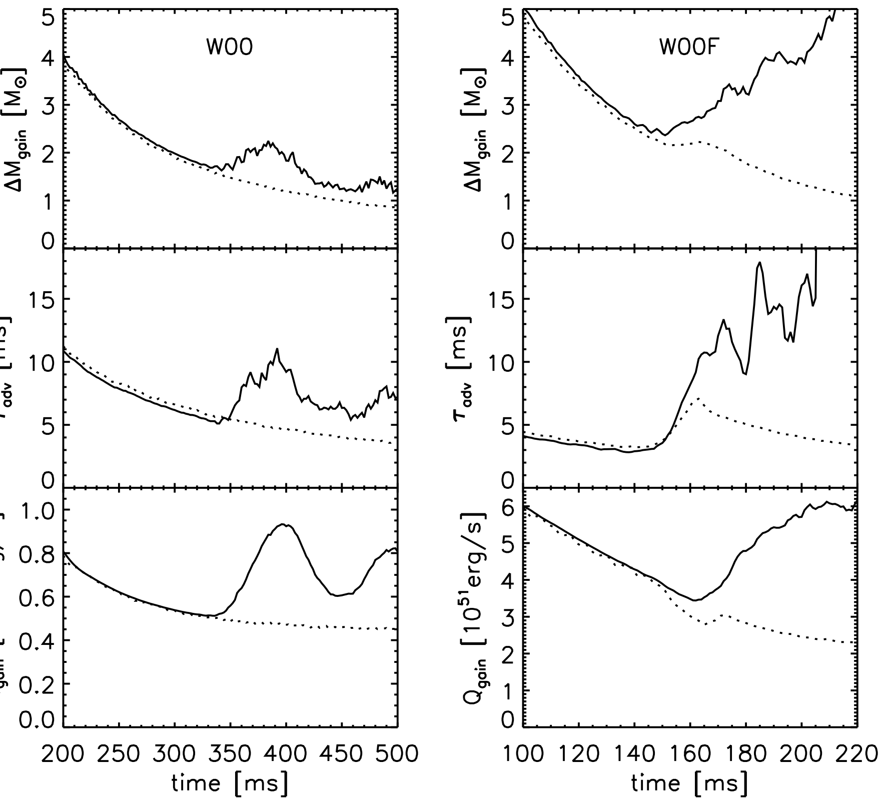

Fig. 19. Evolution of the mass in the gain layer, of the advection timescale from the shock to the gain radius, and of the neutrino heating rate integrated over the whole gain layer for Models W00 and W00F (solid lines). The dotted lines are results from corresponding one-dimensional simulations. When the SASI becomes nonlinear ($t \approx 350$ ms for W00, $t \approx 150$ ms for W00F) and triggers convection (about 30 ms later), the advection timescale and the mass in the gain layer begin to grow. As a consequence, the heating rate increases significantly compared to the one-dimensional simulations. In case of Model W00F the enhanced heating is sufficiently strong to gravitationally unbind the matter in the gain layer and to drive an explosion. The advection timescale shows an increase also in the 1D counterpart of Model W00F at $t \approx 150$ ms, because a composition interface of the progenitor star falls through the shock at this time and the strong decrease of the mass accretion rate leads to a transient expansion of the shock and of the gain layer. Nevertheless the 1D model does not develop an explosion because without the aid of multi-dimensional effects neutrino heating cannot become sufficiently powerful. In Model W00 the neutrino energy deposition rate is so low that even an increase by almost a factor of two between 350 ms and 400 ms is not sufficient for an explosion.

thus exposed to efficient neutrino heating in the vicinity of the gain radius, on the other hand because high-entropy, neutrino-heated matter becomes buoyant, expands quickly, and thus cools, which reduces the energy loss by the reemission of neutrinos. The former of these two effects effectively leads to an increase of the advection timescale of accreted matter from the shock to the gain radius (see also Buras et al. 2006b), as a consequence of which the mass in the gain layer becomes larger. The same effect can also be produced by large-amplitude SASI oscillations, because such non-radial motions expand the average shock radius, thus leading to smaller postshock velocities, and deflect the postshock flow in non-radial direction, also leading to a longer advection time of accreted matter through the gain layer.

In Model W00F we observe such a rise of the advection timescale starting at $t \approx 150$ ms (Fig. 19) when the postshock flow becomes strongly non-radial, but violent convective overturn has not yet set in (Fig. 6, right middle panel). This increase of the advection time leads to a significant growth of the integrated neutrino heating rate in the gain layer, an effect that becomes even more pronounced when the convective activity gains strength ($t \gtrsim 170$ ms). Initially the total specific energy of most of the matter in the gain region is in a narrow range around -11 MeV per nucleon, but the distribution of specific particle energies becomes broader by the influence of the large-amplitude SASI and of convective overturn (Fig. 20). Due to the large energy deposition by neutrinos the mean value of the total energy rises and ultimately some fraction of the matter in the gain layer acquires positive total energy and the explosion sets in. Also in Model W00 we see enhanced neutrino heating (up to two times higher than in the corresponding one-dimensional simulation) from $t \approx 350$ ms on, caused by a combination of nonlinear SASI motions and convective activity (Fig. 19). However, due to the low accretion rate at this late time the neutrino luminosity and thus the neutrino heating rate are much lower than in Model W00F at $t \approx 200$ ms. The total energy in the gain layer of Model W00 increases only temporarily by about 1 MeV per nucleon but then drops again soon and continues to decrease slowly later on (Fig. 20). The distribution of specific energies of matter in the gain layer does not become very broad and none of the matter gets unbound. In both the Models W00 and W00F the specific kinetic energy in the gain layer remains relatively small (only about 1 MeV/nucleon, see Fig. 20).

Different from Blondin et al. (2003) we do not observe a continuous increase of the kinetic energy associated with lateral (turbulent) motion of the matter behind the shock. In their simulations without neutrino effects, Blondin et al. (2003) ob-

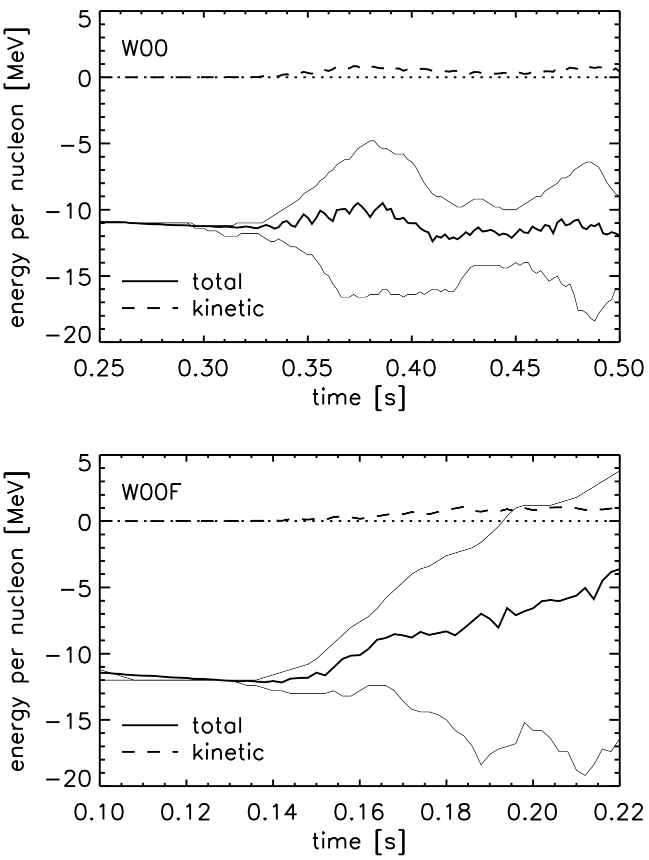

Fig. 20. Average total (kinetic plus internal plus gravitational) energy per baryon (thick solid line) and kinetic energy per baryon (dashed line) versus time in the gain layer of Models W00 and W00F. The thin solid lines correspond to the energy interval that contains 90% of the mass of the gain layer.

served that the SASI oscillation can redistribute some of the gravitational binding energy of the accreted matter from coherent fluid motion to turbulent energy, in fact with sufficient efficiency to drive an expansion of the accretion shock. Since some of the turbulent material had obtained positive total energy at the end of their simulations, Blondin et al. (2003) concluded that the SASI in their calculations was able to lead to an explosion. We do not see this kind of process going on in our simulations. The reason for this discepancy may be the inclusion of neutrino heating and cooling in our models. It is possible that the energy loss by neutrino emission below the gain radius prevents the efficient conversion of gravitational binding energy to turbulent energy. Another reason may be the use of different conditions at the inner grid boundary in our models; while Blondin et al. (2003) assumed steady-state accretion and thus employed a free outflow condition at their inner grid boundary, we follow the accretion and settling of matter onto the forming neutron star due to neutrino cooling and use a closed inner boundary that follows the retreating motion of a Lagrangian mass shell.

In our simulations a growth of the turbulent kinetic energy of the matter in the gain layer is definitely not the reason for starting the explosions. The corresponding lateral kinetic energy never exceeds a few 10^{49} erg in any of our simulations. This is well below the size of neutrino energy deposition and of the energy needed for unbinding matter and triggering an explosion. Nevertheless, the non-radial flow associated with the SASI is certainly helpful, in combination with convection actually crucial for making the neutrino-heating mechanism work. The failure of one-dimensional simulations with the same treatment of the neutrino physics clearly demonstrates the importance of non-radial fluid instabilities, convection and the SASI, for a success of the neutrino-driven explosion mechanism. These hydrodynamic instabilities affect the gas motion in the gain layer such that the advection timescale from the shock to the gain radius is effectively increased. This enhances the efficiency of neutrino energy deposition by allowing more matter to be exposed to the intense neutrino flux near the gain radius for a longer time. Thus both convection and the SASI can be considered as "catalysts" that facilitate neutrino-driven explosions rather than being direct drivers or energy sources of the explosion. As a consequence, explosions in multi-dimensional simulations, i.e. even with the support by convective overturn and the SASI, still require the presence of sufficiently strong neutrino heating. Our set of simulations clearly demonstrates that only in case of a sufficiently large neutrino luminosity and thus only for sufficiently powerful neutrino heating behind the shock, the models are able to develop an explosion. This finding is in agreement with the results of Ohnishi et al. (2006), who also obtained an explosion by neutrino heating only in a simulation with high neutrino luminosity, while lower-luminosity cases failed to explode.

6.3. The importance of the seed perturbations

The comparison of our results shows that explosions during the first second after core bounce do not only require the neutrino luminosities to be sufficiently large but also that the SASI and convection are able to reach the nonlinear phase sufficiently quickly. Whether this is the case or not depends on their growth rates, which in turn depend on the properties of the postshock flow. The latter are a complex function of the progenitor structure, the neutron star contraction, and neutrino cooling and heating in the layer between neutron star and shock. Last but not least, also the size of the seed perturbations, i.e. the inhomogeneities present in the collapsing star, can play a role for the development and growth of non-radial hydrodynamic instabilities after core bounce.

In our Models W12F and W12F-c (as well as in most of the recent simulations with multi-energy group neutrino transport by Buras et al. 2006a,b) the advection time through the gain layer is so short and the growth rate of convective instabilities (Eq. 1) in that region so small that the timescale ratio χ of Eq. (5) remains below the critical threshold χ_0 for a linear growth of globally unstable modes, i.e., $\chi < \chi_0 \approx 3$ according to Foglizzo et al. (2006), see Eq. (6) and also Fig. 3 in Buras et al. (2006b). This means that the fast advection of the flow from the shock to the gain radius suppresses the growth of convective modes according to linear stability analysis. However, as explained in Sect. 2.1, in this case buoyancy can nevertheless drive bubble rise and convective instability in a nonlinear way if the initial density perturbations δ in matter falling through the shock are sufficiently large, i.e. $\delta > \delta_{\rm crit}\exp(-\chi)$ according to Eq. (9), with $\delta_{\rm crit}$ being typically of the order of some percent (see Eq. (8)).

The inhomogeneities in the matter upstream of the shock originate from seed perturbations in the progenitor star, whose size and amplitude are not well known because three-dimensional, long-time stellar evolution simulations for full-sphere models until the onset of core collapse have not been possible so far (see, e.g., Bazan & Arnett 1998; Murphy et al. 2004; Young et al. 2005). With our assumed initial inhomogeneities in case of Models W12F and W12F-c (see Table 1 and Sect. 3.2), the perturbation amplitudes remain below the critical value $\delta_{\rm crit}$ in the former case, whereas they become larger than this threshold value in the latter case (see Fig. 4). Therefore, as visible in Fig. 8, the fastest growing non-radial instability on large scales is the SASI in Model W12F, whereas it is convective overturn in Model W12F-c. Only because of the growth of SASI modes does Model W12F also develop convective activity in the gain layer, which enhances the efficiency of neutrino energy deposition and finally leads to an explosion also in this case. The crucial role of these non-radial instabilities is demonstrated again by a corresponding one-dimensional simulation that does not develop an explosion. In Model W12F the SASI is a key feature in the multi-dimensional evolution, because the development of convective modes is not possible in the first place due to the low initial amplitude of perturbations and the insufficient growth of these perturbations in the advection flow from the shock to the gain radius.

Considering Models W12F and W12F-c, however, no noticeable memory of the initial source of the low-mode asymmetries is retained during the long-time evolution. Although the early postbounce evolution of these two models is clearly different and the times of the onset of the explosion differ, the global parameters of the explosion become very similar (see Table 1). Neither the explosion energy nor the neutron star mass and kick velocity are strongly affected by the different explosion times, because the conditions in the infalling stellar core change only on longer timescales and the ejecta energy and neutron star recoil build up over a much more extended period of time after the launch of the explosion (see Paper I). Since the anisotropies develop chaotically and in a very irregular way during the nonlinear phase, the final ejecta morphology is the result of a stochastic process and does not depend in a deterministic and characteristic manner on the type of non-radial instability that has grown fastest after core bounce. It therefore seems unlikely that observational parameters of supernova explosions are able to provide evidence of the initial trigger of the large-scale anisotropies that develop in the early stages of the explosion. Future simulations with a more detailed treatment of the neutrino transport (instead of our approximative description) and without the use of the inner boundary condition of the present models will have to show whether the gravitational-wave and neutrino signals carry identifiable fingerprints of this important aspect of supernova dynamics.

7. Summary and conclusions

We performed a set of two-dimensional hydrodynamic simulations with approximative neutrino transport to investigate the role of non-convective instabilities in supernova explosions. As initial data we used a postbounce model of a 15 $M_\odot$ progenitor star, which had been evolved through core collapse and bounce in a computation with detailed, energy-dependent neutrino transport. For following the subsequent, long-time evolution, the neutron star core (above a neutrino optical depth of about 100) was excised and replaced by a contracting Lagrangian inner boundary that was intended to mimic the behavior of the shrinking, nascent neutron star. The models of our set differed in the choice of the neutrino luminosities assumed to be radiated by the excised core, in the prescribed speed and final radius of the contraction of the neutron star, and in the initial velocity perturbations imposed on the 1D collapse model after bounce.

Our hydrodynamic simulations indeed provide evidence — supporting previous linear analysis (Foglizzo et al. 2006, 2007; Yamasaki & Yamada 2007) — that two different hydrodynamic instabilities, convection and the SASI (Blondin et al. 2003), occur at conditions present during the accretion phase of the stalled shock in collapsing stellar cores and lead to large-scale, low-mode asymmetries. These non-radial instabilities can clearly be distinguished in the simulations by their growth behavior, location of development, and spatial structure. While convective activity grows in a non-oscillatory way and its onset can be recognized from characteristic mushroom-type structures appearing first in regions with steep negative entropy gradients, the SASI starts in an oscillatory manner, encompasses the whole postshock layer, and leads to low-mode shock deformation and displacement.

As discussed by Foglizzo et al. (2006), the growth of convection is suppressed in the accretion flow because of the rapid infall of the matter from the shock to the gain radius, unless either neutrino heating is so strong and therefore the entropy gradient becomes so steep that the advection-to-growth timescale ratio (χ of Eq. (5)) exceeds the critical value $\chi_0 \approx 3$, or, alternatively, sufficiently large density perturbations in the accretion flow (cf. Eq. (9)) cause buoyant bubbles rising in the infalling matter. While convective instability is damped by faster infall of accreted matter, the growth rate of the SASI *increases* when the advection timescale is shorter. Moreover, the quasi-periodic shock expansion and contraction with growing amplitude due to the SASI produce strong entropy variations in the postshock flow, which can then drive convective instability. Even when the neutrino-heated layer is not unstable to convection in the first place, the perturbations caused by the SASI oscillations can thus be the trigger of "secondary" convection.

Our detailed analysis of the evolution of the SASI modes in our simulations, of their dependence on the model parameters, and of the cooperation between convection and the SASI in the nonlinear regime revealed the following facts:

1. In the linear regime of the SASI the structure of the pressure perturbations reveals an important role of the radius R_∇, where the deceleration of the accretion flow is strongest.

This radius is located in the neutrino-cooling layer somewhat outside the neutrinosphere. The strong deceleration there induces an efficient coupling of vorticity and acoustic perturbations.

2. The period of the low-mode SASI oscillations, whose growth is preferred, scales with the advection time from the shock to R_∇, and not with the sound crossing time through the shock cavity. This result strongly supports the suggestion that the amplification of the SASI happens through an advective-acoustic cycle (AAC) rather than a purely acoustic mechanism.
3. Neutrino heating and cooling do not only play an important role for the supernova explosion mechanism but also for the formation of the coupling zone of vorticity and acoustic perturbations around R_∇ and for the efficiency of the AAC as expressed by the cycle amplification factor $Q_{\rm aac}$.
4. The growth rate of the AAC depends sensitively on the advection time from the shock to the coupling region and the structure of the flow in this region. The latter, in turn, depends on the neutron star contraction, on the neutrino luminosities and the corresponding heating and cooling, and on the mass accretion rate of the stalled shock in the collapsing star. For a wide range of investigated conditions (changing the parameters of our models), we found the AAC being able to develop large amplitudes on timescales relevant for the explosion. Therefore the SASI turned out to create large-scale anisotropy also in cases where convective activity was not able to set in in the first place.
5. When the SASI reaches large amplitudes and supersonic lateral velocities occur in the postshock flow, leading to the formation of sheets with very steep unstable entropy gradients, low-mode convective overturn grows in a highly nonlinear way. Since the SASI and strong convective activity push the accretion shock to larger radii, thus reducing the infall velocity in the postshock layer, and the flow in the neutrino-heating region develops large non-radial velocity components, the accreted matter stays in the gain layer for a longer time. This increases the energy deposition by neutrinos in this region and facilitates the explosion. However, like convection the SASI does not guarantee an explosion on the timescale considered in our simulations: the kinetic energy associated with the SASI remains negligible for the explosion energetics. Therefore sufficiently strong neutrino heating and consequently a sufficiently large neutrino luminosity are still necessary to obtain explosions.
6. In our simulations we could clearly identify a faster contraction and a smaller radius of the excised core of the nascent neutron star as helpful for an explosion. We therefore conclude that a softer high-density equation of state and general relativity, which both lead to a more compact neutron star, are favorable for an explosion. This is so because on the one hand the accretion luminosities of neutrinos become higher, correlated with stronger neutrino heating behind the stalled shock, and on the other hand the growth rate of the AAC increases with a faster advection of matter through the gain layer. Since the initial growth of convection is damped or suppressed by more rapid infall, the presence of the SASI instability and its ability to trigger convection as a secondary phenomenon, play a crucial role for the final success of the delayed neutrino-heating mechanism.
7. The amplitude of the initial seed perturbations in the collapsing core of the progenitor star, which is not well constrained due to the nonexistence of fully consistent and long-evolved three-dimensional stellar evolution models, has an influence on the question whether convection or the SASI develop more rapidly after core bounce. While this can determine how fast the explosion sets in, we found that once the two non-radial instabilities are simultaneously present and cooperate in the nonlinear regime, the global properties of the explosions are essentially insensitive to the initial phase. Since the final anisotropic distribution of the ejecta is the result of a very stochastic and chaotic process, it has also lost the memory of the early evolution. Neither the explosion energy nor the neutron star kick velocity are therefore good indicators of the initial seed perturbations that existed in the progenitor star and of the type of the fastest growing non-radial instability. Future supernova models without the approximations used in our simulations will have to show whether the neutrino and gravitational-wave signals, which will be measurable in detail from a galactic event, carry any useful information about this crucial aspect of the postbounce explosion dynamics.

While the presented simulations employed a number of approximations like the neutrino transport scheme and the use of an inner boundary condition instead of following the evolution of the neutron star core, we are confident that our main findings do not depend on these simplifications. In fact, recent long-time stellar core-collapse simulations with detailed, multi-energy-group neutrino transport and fully consistent consideration of the central part of the nascent neutron star basically confirm the importance of the SASI and its nonlinear interaction with convective instability for the viability of the delayed neutrino-driven explosion mechanism (Marek et al., in preparation).

Acknowledgements. We thank R. Buras and M. Rampp for providing us with post-bounce models and S. Woosley and A. Heger for their progenitor models. Support by the Sonderforschungsbereich 375 on "Astroparticle Physics" of the Deutsche Forschungsgemeinschaft in Garching and funding by DAAD (Germany) and Egide (France) through their "procope" exchange program are acknowledged. The computations were performed on the IBM p655 of the Max-Planck-Institut für Astrophysik and on the IBM p690 clusters of the Rechenzentrum Garching and of the John-von-Neumann Institute for Computing in Jülich.

References

Arcones, A., Janka, H.-Th., & Scheck, L. 2006, A&A, in press, astro-ph/0612582

Arzoumanian, Z., Chernoff, D. F., & Cordes, J. M. 2002, ApJ, 568, 289

Bazan, G. & Arnett, W. D. 1998, ApJ, 496, 316

Blondin, J. M. & Mezzacappa, A. 2006, ApJ, 642, 401

Blondin, J. M., Mezzacappa, A., & DeMarino, C. 2003, ApJ, 584, 971

Buras, R., Rampp, M., Janka, H.-T., & Kifonidis, K. 2003, Phys. Rev. Lett., 90, 241101

Buras, R., Rampp, M., Janka, H.-T., & Kifonidis, K. 2006a, A&A, 447, 1049

Buras, R., Janka, H.-T., Rampp, M., & Kifonidis, K. 2006b, A&A, 457, 281

Burrows, A., Hayes, J., & Fryxell, B. A. 1995, ApJ, 450, 830

Burrows, A., Livne, E., Dessart, L., Ott, C. D., & Murphy, J. 2006, ApJ, 640, 878

Burrows, A., Livne, E., Dessart, L., Ott, C. D., & Murphy, J. 2007, ApJ, 655, 416

Chandrasekhar, S. 1961, Hydrodynamic and hydromagnetic stability (New York: Dover)

Chatterjee, S., Vlemmings, W. H. T., Brisken, W. F., et al. 2005, ApJ, 630, L61

Colella, P. & Woodward, P. R. 1984, J. Comput. Phys., 54, 174

Cordes, J. M., Romani, R. W., & Lundgren, S. C. 1993, Nature, 362, 133

Foglizzo, T. 2001, A&A, 368, 311

Foglizzo, T. 2002, A&A, 392, 353

Foglizzo, T., Scheck, L., & Janka, H.-T. 2006, ApJ, 652, 1436

Foglizzo, T., Galletti, P., Scheck, L., & Janka, H.-T. 2007, ApJ, 654, 1006

Foglizzo, T. & Tagger, M. 2000, A&A, 363, 174

Galletti, P. & Foglizzo, T. 2005, in Proc. SF2A-2005: Semaine de l'Astrophysique Francaise, Strasbourg, France, June 27–July 1, 2005, eds. F. Casoli, T. Contini, J. M. Hameury, & L. Pagani, EdP-Sciences, Conference Series, 2005, p. 487

Hansen, B. M. S. & Phinney, E. S. 1997, MNRAS, 291, 569

Herant, M. 1995, Phys. Rep., 256, 117

Herant, M., Benz, W., Hix, W. R., Fryer, C. L., & Colgate, S. A. 1994, ApJ, 435, 339

Hobbs, G., Lorimer, D. R., Lyne, A.G., & Kramer, M. 2005, MNRAS, 360, 963

Houck, J. C. & Chevalier, R. A. 1992, ApJ, 395, 592

Janka, H.-T. & Müller, E. 1994, A&A, 290, 496

Janka, H.-T. & Müller, E. 1995, ApJ, 448, L109

Janka, H.-T. & Müller, E. 1996, A&A, 306, 167

Kifonidis, K., Plewa, T., Janka, H.-T., & Müller, E. 2003, A&A, 408, 621

Kuhlen, M., Woosley, W. E., & Glatzmaier, G. A. 2003, in ASP Conf. Ser. Vol. 293: 3D Stellar Evolution, eds. S. Turcotte, S. Keller, & R. Cavallo (San Francisco: Astron. Society of the Pacific), 147

Laming, J. M. 2007, ApJ, in press, astro-ph/0701264

Leonard, D. C., Filippenko, A. V., Ganeshalingam, M., et al. 2006, Nature, 440, 505

Liebendörfer, M., Mezzacappa, A., Thielemann, F., et al. 2001, Phys. Rev. D, 63, 103004

Liebendörfer, M., Rampp, M., Janka, H.-T., & Mezzacappa, A. 2005, ApJ, 620, 840

Lyne, A. G. & Lorimer, D. R. 1994, Nature, 369, 127

Murphy, J. W., Burrows, A., & Heger, A. 2004, ApJ, 615, 460

Ohnishi, N., Kotake, K., & Yamada, S. 2006, ApJ, 641, 1018

Rampp, M. & Janka, H.-T. 2002, A&A, 396, 361

Scheck, L., Kifonidis, K., Janka, H.-T., & Müller, E. 2006, A&A, 457, 963

Scheck, L., Plewa, T., Janka, H.-T., Kifonidis, K., & Müller, E. 2004, Phys. Rev. Lett., 92, 011103

Shen, H., Toki, H., Oyamatsu, K., & Sumiyoshi, K. 1998, Nucl. Phys. A, 637, 435

Thompson, C. 2000, ApJ, 534, 915

Thompson, T. A., Burrows, A., & Pinto, P. A. 2003, ApJ, 592, 434

Wang, L., Baade, D., Höflich, P., & Wheeler, J. C. 2003, ApJ, 592, 457

Wang, L., Howell, D. A., Höflich, P., & Wheeler, J. C. 2001, ApJ, 550, 1030

Wang, L., Wheeler, J. C., Höflich, P., et al. 2002, ApJ, 579, 671

Woodward, P. R., Porter, D. H., & Jacobs, M. 2003, in ASP Conf. Ser. Vol. 293: 3D Stellar Evolution, eds. S. Turcotte, S. Keller, & R. Cavallo (San Francisco: Astron. Society of the Pacific), 45

Woosley, S. E. & Weaver, T. A. 1995, ApJS, 101, 181

Yamasaki, T. & Yamada, S. 2007, ApJ, 656, 1019

Young, P. A., Meakin, C., Arnett, D., & Fryer, C. L. 2005, ApJ, 629, L101

Zou, W. Z., Hobbs, G., Wang, N., et al. 2005, MNRAS, 362, 1189